Annu. Rev. Earth Planet. Sci. 2004. 32:111–49
doi: 10.1146/annurev.earth.32.082503.144359

First published online as a Review in Advance on February 3, 2004

GLOBAL GLACIAL ISOSTASY AND THE SURFACE OF THE ICE-AGE EARTH: The ICE-5G (VM2) Model and GRACE

W.R. Peltier
Department of Physics, University of Toronto, Toronto, Ontario, Canada M5S 1A7; email: peltier@atmosp.physics.utoronto.ca

Key Words glacial isostasy, mantle viscosity, ice-age ice sheets, paleotopography

■ **Abstract** The 100 kyr quasiperiodic variation of continental ice cover, which has been a persistent feature of climate system evolution throughout the most recent 900 kyr of Earth history, has occurred as a consequence of changes in the seasonal insolation regime forced by the influence of gravitational n-body effects in the Solar System on the geometry of Earth's orbit around the Sun. The impacts of the changing surface ice load upon both Earth's shape and gravitational field, as well as upon sea-level history, have come to be measurable using a variety of geological and geophysical techniques. These observations are invertible to obtain useful information on both the internal viscoelastic structure of the solid Earth and on the detailed spatiotemporal characteristics of glaciation history. This review focuses upon the most recent advances that have been achieved in each of these areas, advances that have proven to be central to the construction of the refined model of the global process of glacial isostatic adjustment, denoted ICE-5G (VM2). A significant test of this new global model will be provided by the global measurement of the time dependence of the gravity field of the planet that will be delivered by the GRACE satellite system that is now in space.

INTRODUCTION

Although the term isostasy was first coined by Dutton (1889) to describe the apparently "compensated" state of Earth's surface topography, the idea that such compensation must occur dates from the studies performed by both Airy (1855) and Pratt (1855) based upon observations of plumb line deflections made during the original geodetic survey of India (e.g., see Keay 2000 for a fascinating account of the history of the making of these epochal measurements). Although originally intended, therefore, to refer to the compensation of observed external loads (mountains) by unobservable internal density heterogeneity (their roots), the term isostasy applies equally well to the compensation of applied external surface loads (continental glaciers and ice sheets) by variations in Earth's external shape and internal density distribution. Although we cannot observe the time dependence of

the process whereby compensation is achieved in the case of the surface topography of the solid Earth, it having been established in the remote past through the action of processes acting over long timescales, the same is not true of the process of glacial isostasy. It is extremely fortunate from the perspective of both solid Earth geodynamics and (paleo) climate dynamics that the most recent global deglaciation event, which marked the end of the most recent 100 kyr ice-age cycle of the late Quaternary period, began only 21,000 calendar years ago. Because this period of time lies squarely in the range in which radioactive carbon (^{14}C) dating is applicable to provide chronological control on the geological system within which the planetary response to this event has been recorded, extremely high quality quantitatively constrained analyses may be performed using detailed mathematical models of the process. Although such analyses have, for the most part, been performed in support of geophysical inferences of the effective viscosity of the mantle of Earth (Haskell 1935, Niskanen 1939, McConnell 1968, Cathles 1975, Peltier 1974), more recently, the focus has been extended to include the application of the same mathematical models to infer the thicknesses of the distinct ice sheets that were in place at the Last Glacial Maximum (LGM), which occurred approximately 21,000 years ago (Peltier 1994, 1996, 2002c). This review discusses recent progress in both of these facets of the inverse problem posed by the observations related to the glacial isostatic adjustment (GIA) process.

The importance of the mantle viscosity aspect of GIA analyses derives from the fact that this is one of the few methods whereby one may interrogate the (steady-state?) creep resistance of the deep mantle (e.g., see Peltier 1974, Karato & Wu 1993, Peltier 1998a, Butler & Peltier 2002). Because the magnitude of this creep resistance is a required ingredient in the construction of a priori models of the mantle convection process that is responsible for continental drift and sea-floor spreading, it is clear that understanding of the process of glacial isostatic adjustment must constitute a major component of the edifice of quantitative geodynamics. Less clear, until recently, has been the important role that the understanding of this phenomenon might play in refining our knowledge of the amount and detailed distribution of land ice that existed on the continents at LGM. Although the position of the margins of the primary concentrations of land ice at that time has been reasonably well known (with a critical exception discussed below) on the basis of many decades of concerted effort in the area of glacial geomorphology, the thicknesses of these ice sheets have been only weakly constrained on the basis of reconstructions derived from the application of equilibrium glaciological models of continental ice-sheet form. A significant recent advance, which is reviewed herein, has been achieved by applying a combination of the isostatic adjustment and ice mechanical modeling–based methodologies. This has provided a primary means whereby it has proven possible to significantly refine the previous ICE-4G (VM2) model of the GIA process that was presented in Peltier (1994, 1996) and which has since served as the standard model of the phenomenon, especially for the purpose of providing surface boundary conditions for coupled atmosphere-ocean climate model reconstructions of the climate of Earth at LGM [e.g., see Pinot et al.

1999 for a discussion of recent results from the continuing Paleoclimate Modelling Intercomparison Project (PMIP)].

In the following section of this review, I provide a brief discussion of the modern form of the mathematical theory of the glacial isostatic adjustment process, one that focuses upon the several enhancements to this theory that have been introduced in the past decade. The subsequent section provides a discussion of both successes and failures of the ICE-4G (VM2) model. As the failures of the model appear at this time to be related more to the ICE-4G model of the spatiotemporal form of the surface ice load, rather than to the VM2 model of the radial viscoelastic structure, the penultimate section of the paper discusses the modifications to ICE-4G that have been required to fit the new observational constraints that have become available over the course of the past decade since the ICE-4G model was published. This review also includes a number of specific predictions of the signals that the GRACE satellite system should observe if the refined ICE-5G (VM2) model were exact and if the only physical process contributing significantly to the time dependence of geoide height were GIA.

THEORY OF THE GLOBAL PROCESS OF GLACIAL ISOSTATIC ADJUSTMENT AND RELATIVE SEA LEVEL CHANGE

The mathematic structure of the theory of the glacial isostatic adjustment process, a theory that is now in rather general use, was originally developed in a series of papers published in the 1970s (Peltier 1974, 1976; Farrell & Clark 1976; Peltier & Andrews 1976; Clark et al. 1978; Peltier et al. 1978). In this initial form of the theory, the history of relative sea-level (RSL) change, $S(\theta, \lambda, t)$, induced by an assumed known history of glaciation and deglaciation, was predicted as a solution of what I have come to call the sea level equation (SLE), namely

$$S(\theta,\lambda,t) = C(\theta,\lambda,t)\left[\int_{-\infty}^{t} dt' \iint_{\Omega} d\Omega' \, L(\theta',\lambda',t')\, G^{L}(\gamma, t-t') + \frac{\Delta\Phi(t)}{g}\right], \quad (1)$$

in which $S(\theta, \lambda, t)$ is the history of sea-level change relative to the deforming surface of the solid Earth at latitude θ and longitude λ as a function of time t. The function $C(\theta, \lambda, t)$ is the so-called ocean function, which is unity where there is ocean and zero where there is continent. In the earliest work referenced above, this function was assumed to be time independent so that coastlines were kept fixed to their modern forms. A significant advance described in Peltier (1994) was the development of a self-consistent global methodology whereby this assumption could be relaxed. This advance is reviewed below.

The function L in Equation 1 is the surface mass load per unit area, which has the composite form

$$L(\theta, \lambda, t) = \rho_I I(\theta, \lambda, t) + \rho_w S(\theta, \lambda, t), \tag{2}$$

in which ρ_I and ρ_w are ice and water density, respectively, and where I is the spatiotemporal variation of ice thickness. Because the unknown field $S(\theta, \lambda, t)$ appears both on the left-hand side of Equation 1 as well as under the three-dimensional convolution integral, Equation 1 is clearly an integral equation. The "kernel" of the three-dimensional convolution integral, $G^L(\gamma, t)$, is the viscoelastic Green function for the time-dependent separation between the surface of the sea (the geoide of classical geodesy) and the surface of the solid Earth. The argument γ of this function is the angular separation between source point and field point. The methodology employed for the construction of this impulse-response function was described in Peltier (1974) and somewhat further refined in Peltier (1976) and Peltier (1985). Application of this methodology, which is not reviewed in detail here, delivers an expression for $G^L(\gamma, t)$ in the form

$$G^L(\gamma, t) = \frac{a}{me} \sum_{\ell=0}^{\infty} \left(1 + k_\ell^L(t) - h_\ell^L(t)\right) P_\ell(\cos\gamma), \tag{3}$$

in which *a* and *me* are Earth's mean radius and mass, respectively; the P_ℓ are conventional Legendre polynomials; and $k_\ell^L(t)$ and $h_\ell^L(t)$ are the time-dependent viscoelastic equivalents of the constant elastic surface load Love numbers of Farrell (1972). The final term in Equation 1 involves a purely time-dependent function that must be added to Equation 1 in order to ensure that the adjustment process that it describes is mass conserving in the sense that the mass of water produced by the melting of ice of thickness $I(\theta, \lambda, t)$ exactly equals the mass of water that fills the ocean basins. Multiplying Equation 1 by ρ_w and integrating over the (actually time-dependent) surface area of the oceans delivers the following expression for $\Delta\Phi(t)$ (see Peltier 2002a for a recent detailed discussion):

$$\frac{\Delta\Phi(t)}{g} = -\frac{M_I(t)}{\rho_w A(t)} - \frac{1}{A(t)}\langle\chi\rangle, \tag{4}$$

in which $M_I(t)$ is the mass lost (gained) by the ice sheets in melting (accreting) by time t, A(t) is the time-dependent surface area of the oceans, and $\langle\chi\rangle$ is the integral of the triple convolution integral in Equation 1 over the (time-dependent) surface area of the oceans. The inputs to Equation 1 consist of the assumed known glaciation history $I(\theta, \lambda, t)$ and the (assumed known) radial viscoelastic structure that determines the time-dependent viscoelastic Love numbers $k_\ell^L(t)$ and $h_\ell^L(t)$.

Because the variations in surface mass load associated with the process of glaciation and deglaciation are large, such as to account for a change in mean sea level between the glacial and interglacial states of approximately 125 m (see below for a detailed discussion of this new value for the eustatic variation), the moment of inertia tensor of the planet is significantly influenced by the 100 kyr glaciation cycle. The mathematical analysis described in Peltier (1982) and Wu & Peltier (1984) provided the first accurate means of predicting the nature of the

rotational response to the glaciation-deglaciation process, a response that includes not only an induced time dependence in the rate of axial rotation and therefore in the length of day, but also a "wander" of the pole of rotation with respect to the surface geography. These two aspects of Earth's rotational state are both observable, the first in terms of the time dependence in the degree two and order zero Stokes coefficient in the expansion of the gravitational field of the planet (usually denoted $\dot{J}_2$; the first measurement of which was reported by Yoder et al. 1983; see Cox & Chao 2002 and Dickey et al. 2002 for more recent discussions), and the second in terms of the path of the pole measured using the array of photo-zenith tubes that constituted the main source of data employed by the International Latitude Service (ILS) (Vincente & Yumi 1969, 1970) or using very long baseline radio-interferometry (VLBI) (see e.g., Carter et al. 1986 for the earliest application of this methodology to the GIA problem). Peltier (1982, 1983) showed that the satellite observed $\dot{J}_2$ was explicable as a consequence of the glacial isostatic adjustment process, as were the observed speed and direction of true polar wander evident in the ILS pole path. That the GIA explanation for both of these anomalies in Earth's rotational state is correct, notwithstanding the additional minor contributions that must be due to other influences, is strongly suggested by the fact that these entirely independent observations are reconciled by the same model(s) of the radial viscoelastic structure of the planet. This fact has been stressed recently in Peltier (1998b). Mitrovica & Peltier (1993) presented the first detailed theoretical calculations of all of the low-degree time-dependent zonal Stokes coefficients based upon the ICE-3G deglaciation model of Tushingham & Peltier (1991), and Cheng et al. (1989) have tabulated all of these that can be inferred on the basis of satellite laser ranging (SLR) observations.

Because changes in the rotational state of the planet are accompanied by changes in the centrifugal potential, and because sea level is equally influenced by changes in this contribution to the potential as by changes owing to the redistribution of mass, it should be clear that there must be an additional impact upon sea-level history owing to the changing rotation. This influence may be included in Equation 1 by modifying it into the form

$$S(\theta, \lambda, t) = C(\theta, \lambda, t) \left[\int_{-\infty}^{t} dt' \iint_{\Omega} d\Omega' \{ L(\theta', \lambda', t') G^{L}(\gamma, t - t') + T(\theta', \lambda', t') G^{T}(\gamma, t - t') \} + \frac{\Delta \Phi(t)}{g} \right]. \quad (5)$$

In this equation, $T(\theta, \lambda, t)$ is the change of the centrifugal potential owing to the changing rotation, a function that may be constructed following Dahlen (1976) to obtain a solution in the form of the following spherical harmonic expansion:

$$T(\theta, \lambda, t) = T_{oo}(t) Y_{oo}(\theta, \lambda) + \sum_{m=-1}^{+1} T_{2m} Y_{2m}(\theta, \lambda), \quad (6)$$

with

$$T_{oo}(t) = \frac{2}{3}\omega_3(t)\Omega_o a^2, \tag{7a}$$

$$T_{20}(t) = \frac{-1}{3}\omega_3(t)\Omega_o a^2\sqrt{4/5}, \tag{7b}$$

$$T_{2,+1} = (\omega_i(t) - i\omega_2(t))\big(\Omega_o a^2/2\big)\sqrt{2/15}, \quad \text{and} \tag{7c}$$

$$T_{2,-1} = -(\omega_i(t) + i\omega_2(t))\big(\Omega_o a^2/2\big)\sqrt{2/15}. \tag{7d}$$

In Equations 7a–d, the $\omega_i(t)$ are the individual Cartesian components of the time dependence of angular velocity of the planet induced by the glaciation-deglaciation process, whereas Ω_o is the axial angular velocity in the unperturbed state. Peltier (1999) pointed out that it was important to include only terms of first order in the $\omega_i(t)$ in Equation 6 because the theory of Peltier (1982) and Wu & Peltier (1984) used to compute these terms was a theory that was accurate only to this order.

Of course changes in Earth's rotational state feedback not only upon sea level but also upon all other aspects of the planet's response to glaciation and deglaciation. In particular, the full three-dimensional displacements of points on Earth's surface, which are now being measured using the global positioning system (GPS) (see Tarasov & Peltier 2002 and Johansson et al. 2002) and VLBI (see Argus et al. 1999) techniques, may be predicted, following the solution of Equation 5 for a specific model of surface loading and for a specific model of the radial viscoelastic structure, by evaluating a convolution integral of the full surface load, $L = \rho_I I + \rho_w S$, with an appropriate Green function. Such convolution integrals may be most accurately evaluated using a spectral representation as in Peltier (1976). For the radial displacement scalar and the tangential displacement vector, these spectral representations of the solution are simply (e.g., Peltier 2002c)

$$U(\theta,\lambda,t) = \sum_{\ell=o}^{\infty}\sum_{m=-\ell}^{+\ell}\left[\frac{4\pi a^3}{(2\ell+1)me}\left(L_{\ell m}h_\ell^{E,L} + \sum_{k=1}^{K(\ell)} q_k^\ell \beta_{\ell m}^k\right) + \frac{4\pi}{(2\ell+1)g}\left(T_{\ell m}h_\ell^{E,T} + \sum_{k=1}^{K(\ell)} q_k'^E \beta_{\ell m}'^K\right)\right] Y_{\ell m} \tag{8a}$$

$$\underline{V}(\theta,\lambda,t) = \sum_{\ell=o}^{\infty}\sum_{m=-\ell}^{+\ell}\left[\frac{4\pi a^3}{(2\ell+1)me}\left(L_{\ell m}\ell_\ell^{E,L} + \sum_{k=1}^{K(\ell)} t_k^\ell \beta_{\ell m}^k\right) + \frac{4\pi}{(2\ell+1)g}\left(T_{\ell m}\ell_\ell^{E,T} + \sum_{k=1}^{K(\ell)} t_k'^E \beta_{\ell m}'^k\right)\right] \underline{\nabla} Y_{\ell m}. \tag{8b}$$

In Equations 8a,b, the parameters q_k^ℓ, $q_k'^\ell$, t_k^ℓ, and $t_k'^\ell$ are the residues at the poles s_k^ℓ that appear in the viscoelastic normal mode theory of the glacial isostatic

adjustment process of Peltier (1974, 1976, 1985), whereas the $h_\ell^{E,L}$, $h_\ell^{T,L}$, $\ell_\ell^{E,L}$, and $\ell_\ell^{E,T}$ are the elastic asymptotes of the h and ℓ Love number spectra for surface mass (L) and centrifugal potential (T) loading, respectively. The functions $\beta_{\ell m}$ and $\beta'_{\ell m}$ are, as defined in Wu & Peltier (1982),

$$\beta_{\ell m}^{k} = \int_{-\infty}^{t} L_{\ell m}(t) e^{-s_k^{\ell}(t-t')}\, dt' \quad \text{and} \tag{9a}$$

$$\beta_{\ell m}^{\prime k} = \int_{-\infty}^{t} T_{\ell m}(t) e^{-s_k^{\ell}(t-t')}\, dt', \tag{9b}$$

where the inverse relaxation-time spectrum for surface load and tidal potential load forcing are identical so long as the model of the radial viscoelastic structure is the same.

For the purpose of this review, I focus upon a small subset of models of the radial viscoelastic structure for which the depth dependence of mantle viscosity is shown in Figure 1, where the models are respectively denoted VM1, VM2, and VM3. For each of these models, the radial variation of elastic properties is assumed to be fixed to that in the Preliminary Reference Earth Model (PREM) of Dziewonski & Anderson (1981). The viscoelastic relaxation spectra for these models, from Peltier (1998b), are shown on Figure 2. For each spherical harmonic degree ℓ, these spectra are characterized by a discrete set of inverse relaxation times $s_k^{\ell}[k = 1, \ldots K(\ell)]$, which appear in the Dirichlet series expansions for the time dependence of the h, k, and ℓ Love numbers for both surface load and tidal potential load forcing. For the former, these Love number expansions are, explicitly,

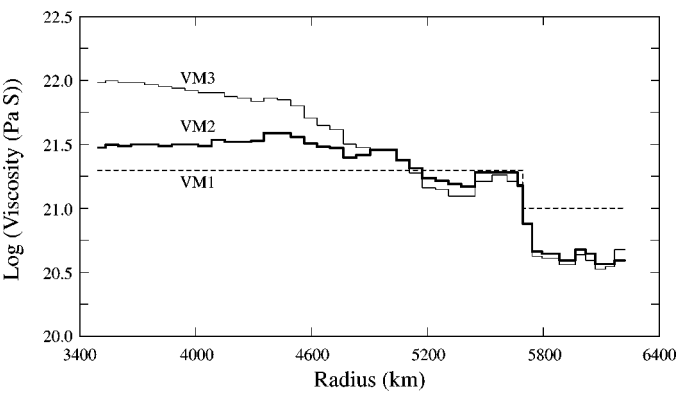

Figure 1 Models of the depth dependence of mantle viscosity to be employed for the purpose of discussion in this review.

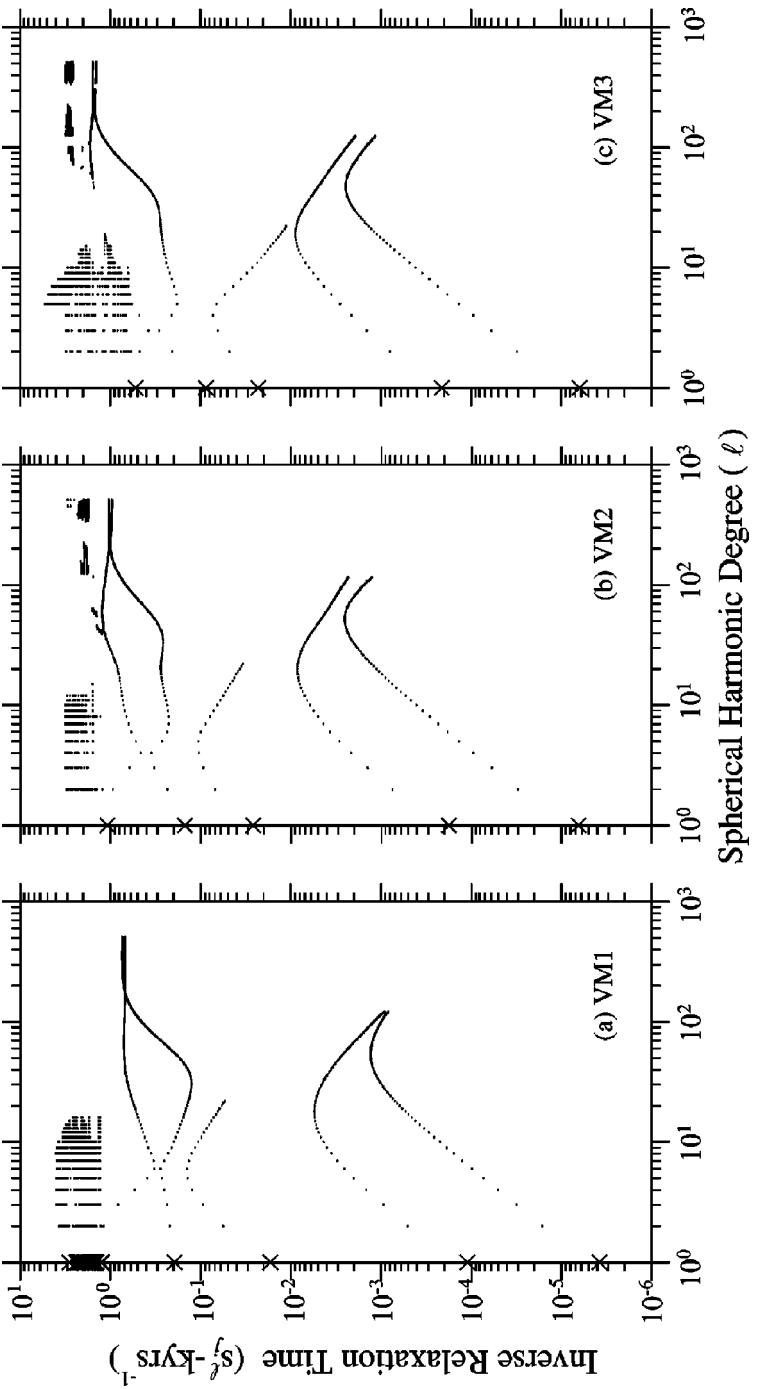

Figure 2 Viscoelastic relaxation spectra for Earth models having the mantle viscosity profiles VM1, VM2, and VM3 shown in Figure 1.

$$h_\ell^L(t) = h_\ell^{L,E}\delta(t) + \sum_{k=1}^{K(\ell)} r_j^\ell e^{-s_j^\ell t}, \tag{10a}$$

$$k_\ell^L(t) = k_\ell^{L,E}\delta(t) + \sum_{k=1}^{K(\ell)} q_j^\ell e^{-s_j^\ell t}, \text{ and} \tag{10b}$$

$$\ell_\ell^L(t) = \ell_\ell^{L,E}\delta(t) + \sum_{k=1}^{K(\ell)} t_j^\ell e^{-s_j^\ell t}, \tag{10c}$$

with analogous expressions for the tidal Love numbers that are required to compute the rotational forcing.

Very recently (Peltier 2002c), it has become possible to confront the global model of the GIA process with other observations related to the GIA process, observations that have led to the ability to significantly refine the functional form $I(\theta, \lambda, t)$ that is employed to describe glaciation history. These observations consist of repeated absolute gravity measurements at sites on the Canadian Shield that were previously ice covered but from which RSL records are unavailable, as the sea never inundated the sites. The instruments that have been employed for this purpose are those designed by James Faller of the University of Colorado (e.g., Faller 1967, 1995, 2002; Faller & Marson 1995; Faller & Vitouchkine 2002) in which the surface value of the gravitational acceleration g is measured by drops of a test mass, the acceleration of which is measured using a laser tracking system. By averaging over a large number of "drops," the acceleration may be determined to high accuracy. Lambert et al. (2001) have employed repeated measurements made using the Faller instruments to measure $\dot{g}$, the time derivative of g at sites along a traverse extending from Churchill on the west coast of Hudson Bay in Canada, into Iowa across the Canada-United States border.

The time dependence of g that is induced by the process of glaciation and deglaciation may be computed by evaluating the convolution integral:

$$\Delta g(\theta, \lambda, t) = \int_{-\infty}^{t} dt' \iint_{\Omega} d\Omega' L(\theta', \lambda', t') G^g(\gamma, t - t'), \tag{11}$$

in which the Green function for the gravity anomaly Δg on the solid surface of Earth, on which the measurements are made, is just (e.g., see Farrell 1972 for the elastic equivalent)

$$G^g(\gamma, t) = \sum_{\ell=o}^{\infty} \left\{ \frac{g}{me}\left(\ell + 2h_\ell^E - [\ell+1]k_\ell^E\right)\delta(t) + \sum_{k=1}^{K(\ell)} \frac{g}{me}\left(2r_k^\ell - [\ell+1]r_k^{\prime\ell}\right)e^{-S_k^\ell t}\right\} P_\ell(\cos\gamma), \tag{12}$$

where the additional terms required to include the contribution owing to rotational feedback are obvious and have been dropped to conserve space. An excellent approximation to the above general solution for Δg follows simply by noting that $\ell k_\ell^E \approx h_\ell^E$ and $\ell r_k'^\ell \approx r_k^\ell$, expressions that are found to be sufficiently accurate for most purposes. In the regime of pure viscous decay when the elastic contribution to the dependence of the field can be neglected, we then have

$$\Delta g(\theta, \lambda, t) \approx \frac{g}{a} \int_{-\infty}^{t} dt' \iint_{\Omega} d\Omega' L(\theta', \lambda', t') G^R(\gamma, t'), \tag{13}$$

where G^R is just the Green function for radial displacement. For the time derivative of g, $\dot{g}$, we therefore have $d\Delta g/dt \approx (g/a)$ d(radial displacement)/dt. Knowing the time dependence of radial displacement computed from Equation 8a, we may therefore predict the time rate of change of the surface gravitational acceleration to reasonable accuracy.

An additional recent advance in the continuing development of the theory of the GIA process concerns the analysis that can be performed in order to predict the time-dependent topography of the landscape with respect to the evolving level of the sea that accompanies the glacial isostatic adjustment process. This aspect of the theory was first developed in Peltier (1994, 1996) and makes use of the fact that the SLE (Equation 5) is a construct of first-order perturbation theory and therefore describes the evolution of the relative level of the sea with respect to an undefined and therefore arbitrary datum. This arbitrariness may be exploited so as to produce a prediction of RSL that I refer to as being topographically self-consistent. This is constructed by computing a field $T'(\theta, \lambda)$ such that

$$S(\theta, \lambda, t_p) + T'(\theta, \lambda) = T(\theta, \lambda, t_p), \tag{14}$$

where $T(\theta, \lambda, t_p)$ is the present day topography of the planet with respect to sea level, defined globally using the highest resolution topographic data set [Digital Elevation Model (DEM)] available. In Equation 12, t_p is the present time. Given the $T'(\theta, \lambda)$ defined by Equation 14, we may then compute

$$T(\theta, \lambda, t) = S(\theta, \lambda, t) + T'(\theta, \lambda) = S(\theta, \lambda, t) + [T_p(\theta, \lambda) - S(\theta, \lambda, t_p)]. \tag{15}$$

At any time for which ice continues to exist on the landscape, we may then compute the full paleotopography by calculating

$$PT(\theta, \lambda, t) = T(\theta, \lambda, t) + I(\theta, \lambda, t). \tag{16}$$

Now, where PT is negative there exists water-covered land (ocean), whereas where PT is positive, there is (perhaps ice-covered) continent. The former region defines the time dependence of the ocean function that appears in Equation 5. To implement this element of the theory, we are obliged to iteratively refine our knowledge of $C(\theta, \lambda, t)$. By working in this way, we are able to construct a full three-dimensional model of the evolution of the global landscape showing the way

in which the land emerges from the sea as postglacial rebound proceeds and the way in which new shorelines are cut into the landscape, shorelines which exist today as memories of this complex interplay of earth, ocean, and ice-related processes.

In the following section of this review, I discuss the quality of the ICE-4G (VM2) model by comparing its predictions to a number of observational constraints, comparisons that address not only the successes of the model but also the failures that have provided the motivation for its improvement. In the subsequent section, ICE-5G (VM2): A Refined Model of the Post-LGM Global Deglaciation Process, the focus is upon the new ICE-5G (VM2) model that has resulted through correction of the flaws in the previous model that have been revealed by these tests.

TESTS OF THE ICE-4G (VM2) MODEL OF THE GIA PHENOMENON

The primary data, on the basis of which one may test models of the GIA process, consist of radiocarbon-dated histories of RSL change through the postglacial period. For the most part, such records consist of time series confined to the Holocene period extending from approximately 10,000 calendar years ago to the present, although there do exist a very few records, primarily those based upon coral sequences from the tropics, that extend further back in time. These records of RSL history provide the most important constraints upon both mantle viscosity and deglaciation history and are the main focus in this section. As our primary focus here is upon the isolation of flaws in the deglaciation history ICE-4G, we begin with a brief recapitulation of tests that have been performed on the radial viscosity structure VM2. After demonstrating that this component of the model is much better constrained than is the ICE-4G component, I focus squarely upon the difficulties recently revealed with the latter.

The VM2 Model of the Radial Viscosity Structure of the Planet

As mentioned previously, we may take it as understood that the viscosity of Earth's mantle could not depend only upon depth because the thermal convection process mixes this region of Earth and because this process is characterized by the occurrence of strong lateral heterogeneity of temperature. Because the creep of a solid is a thermally activated phenomenon, it is clear that lateral temperature heterogeneity must be accompanied by lateral viscosity heterogeneity. By assuming that viscosity depends only upon depth, we may nevertheless test the viability of this assumption insofar as reconciliation of glacial rebound data is concerned. The logical path that I have chosen to follow in conducting this test has involved the exploitation of two fundamental properties of RSL observations. First, there is the property that postglacial rebound data from previously ice-covered regions are sensitive to the properties of the viscoelastic structure over a range of depth that depends upon the horizontal scale of the ice sheet whose removal upon

deglaciation is responsible for inducing the uplift. The second important property of RSL data from such regions is that it is often possible to extract from them a property that depends almost entirely upon viscosity and is essentially independent of errors in deglaciation history. Usually, this property is related to a relaxation time that is characteristic of the time dependence of some aspect of the glacial rebound process. Figure 3, for example (from Peltier 1998b), shows the results obtained by Monte Carlo fits to ^{14}C dated RSL records from the Hudson Bay region in Canada (SE Hudson Bay and James Bay) and from the Gulf of Bothnia in Sweden (Angermanland River). The model fit to the data is a two-parameter exponential model characterized by an amplitude and a relaxation time, values for which are shown in the panels describing the data at the individual locations. Relaxation times are determined primarily by mantle viscosity and vary from approximately 3.4 kyr in SE Hudson Bay to 4.2 kyr in the Gulf of Bothnia. Figure 4 shows a different and complementary set of relaxation time data, that from McConnell

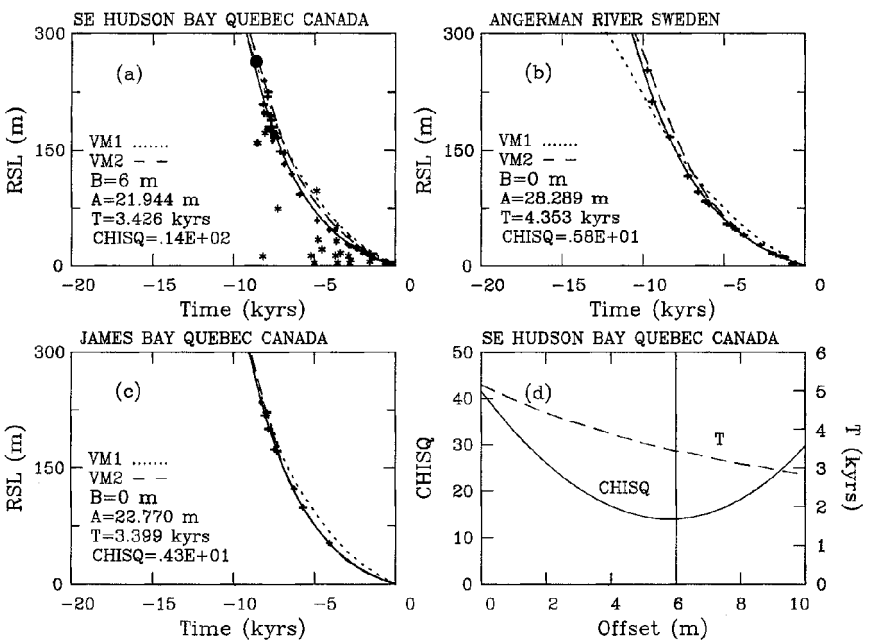

Figure 3 Results for relaxation time T and amplitude A based upon Monte Carlo fits (*solid lines*) to observed RSL data from (*a*) SE Hudson Bay, (*b*) Angermanland River in Sweden, and (*c*) James Bay in Canada. These fits are obtained by first transforming the ^{14}C ages of the samples to sidereal age using the standard INTCAL (Stuiver et al. 1998) procedure. Theoretical predictions based upon the ICE-4G (VM1) and ICE-4G (VM2) models are shown as dotted and dashed lines, respectively. (*d*) Typical result obtained for determination of the "storm beach" offset for wood samples from the southeast Hudson Bay region.

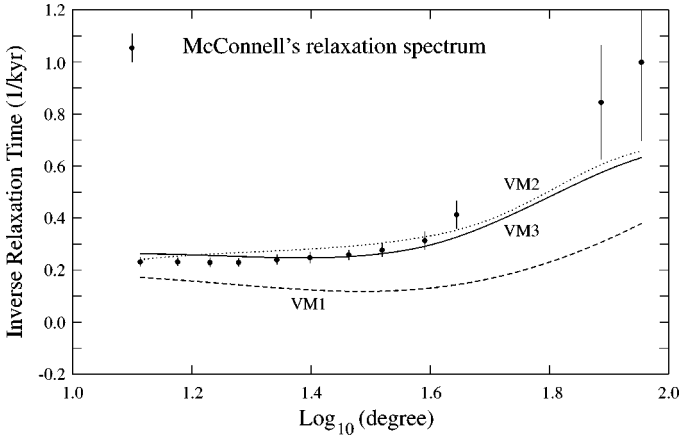

Figure 4 Inverse relaxation time as a function of spherical harmonic degree derived from strand line observations related to the postglacial rebound of Fennoscandia. Comparisons to these data of McConnell (1968) are shown for each of the VM1, VM2, and VM3 viscosity models.

(1968), which assigns a specific relaxation time to each spherical harmonic degree ℓ in the deformation of Earth's surface that continues over the Fennoscandia region. Figure 5 shows a set of Fréchet kernels for the mantle viscosity inverse problem for data of all of the types that were employed in Peltier (1996) in the formal Bayesian inversion that delivered the VM2 model from the VM1 starting model shown on Figure 1. Inspection of this figure, which includes sample Fréchet kernels for several different spherical harmonic degrees for the relaxation times in the McConnell spectrum (based upon the analytical form for these kernels derived in Peltier 1976), for the relaxation times extracted from individual ^{14}C dated RSL histories, and for the previously discussed rotational constraints provided by $\dot{J}_2$ and polar wander speed, demonstrate the fact that these data exhibit sensitivity to viscosity over different ranges of depth. The Fréchet kernels for the latter two types of data must be determined numerically as recently discussed in Peltier (1998a,b). In Peltier (1996), the Bayesian methodology of Tarantola & Valette (1982a,b) was employed to infer the model labeled VM2 on Figure 1 from the starting model labeled VM1.

That VM2 was, in fact, a significant improvement upon VM1 followed from examination of fits to RSL observations that had not been employed to constrain the new model. It was shown in Peltier (1996), in particular, that the new viscosity model entirely removed the large misfits to ^{14}C dated RSL observations from all sites along the U.S. east coast that had been revealed in the analyses by Tushingham & Peltier (1991, 1992) using the VM1 viscosity model. A comparison of the fits of the VM1 and VM2 models to the individual RSL curves in Figure 3 and to the Fennoscandian relaxation spectrum of McConnell in Figure 4 are shown in these

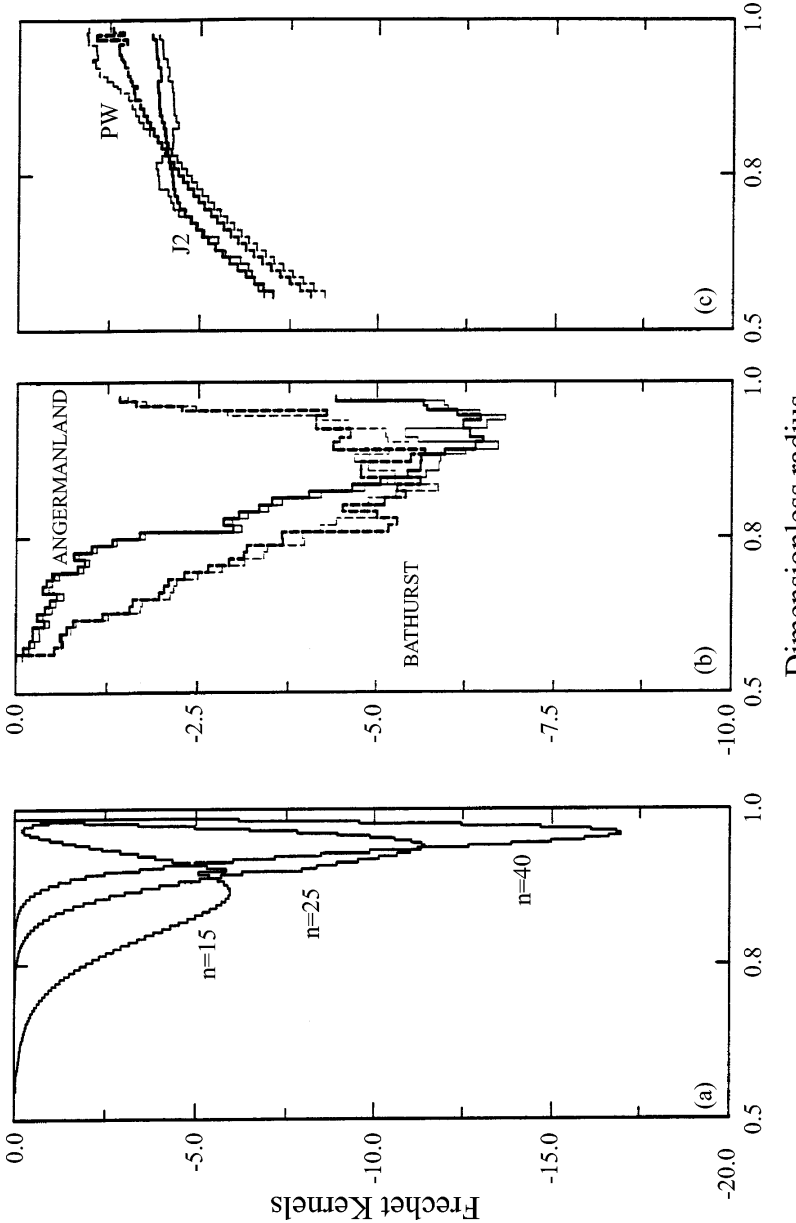

Figure 5 Example Fréchet kernels for the three different types of data employed to infer the depth variation of mantle viscosity (*a*) kernels for individual relaxation times for three different spherical harmonic degrees in the Fennoscandia relaxation spectrum shown on Figure 4, (*b*) kernels for relaxation times extracted from the ^{14}C dated RSL curves at two sites on the Canadian Shield as in Figure 3, (*c*) kernels for nontidal acceleration and polar wander speed.

figures. The high quality of the fit of ICE-4G (VM2) model to the rotational observables is shown on figure 30 of Peltier (1998b). What is very important to note, however, is the sensitivity of the viscosity characteristic of the deepest part of the lower mantle to the precise values for $\dot{J}_2$ and polar wander speed that are attributable to the glacial isostatic adjustment process. As first demonstrated in Peltier & Jiang (1996), Peltier (1996), and Peltier (1998a,b), if it were the case that either the Greenland or Antarctic ice sheets were currently disintegrating at a rate sufficient to produce a significant fraction of the approximately 1.85 mm year^{-1} rate of global sea-level rise that has been inferred on the basis of tide gauge analyses (e.g., see Peltier 2002d), then the viscosity of the deepest mantle would have to be revised upward in order that the satellite observation of $\dot{J}_2$ continue to be reconciled. If the ongoing rate of polar ice-sheet melting were such as to cause the sea level to rise at the rate of 1.5 mm year^{-1}, for example, and the formal inversion of the GIA data repeated taking this "contamination" of the $\dot{J}_2$ observation into account, then the result is the VM3 model of viscosity shown in Figure 1. It is notable that the formal Bayesian inversion that delivered VM3 does not impact the inferred viscosity of the mantle at all at depths shallower than approximately 1500 km. This is clearly a consequence of the fact, obvious by inspection of the Fréchet derivatives shown in Figure 5, that only the rotational data are sensitive to viscosity in this deeper region. The viscosity of the upper part of the lower mantle, and of the overlying transition zone and upper mantle, are "clamped" by the available relaxation time observations. Because modern polar ice-sheet melting at a rate sufficient to raise global sea level by 1.5 mm year^{-1} must be considered an upper bound, given the additional contributions to global sea-level rise owing to the steric effect of thermal expansion of the oceans (see Levitus et al. 2000, 2001 and Munk 2002 for a recent review) and to the melting of small ice-sheets and glaciers (Meier 1984, Dyurgerov & Meier 2000, Arendt et al. 2002), both of which have a current impact that appears to be bounded above by a rate of approximately 0.5 mm year^{-1}, it would appear that the elevation of viscosity in the lowermost lower mantle in the VM3 model is an upper bound for this region of Earth. If one introduces the expected low viscosity layer in the D$''$ region of the mantle adjacent to the core-mantle boundary, however, one need not appeal to strong contamination of $\dot{J}_2$ owing to modern polar ice-sheet melting to maintain high viscosity in the bulk of the lowermost lower mantle.

Recent tests of the viscoelastic structure of the VM2 model at shallowest depth have led to the suggestion that modification of the model may also be necessary in this region. Analyses of the glacial isostatic adjustment of the entire British Isles (Peltier et al. 2002) have demonstrated that the 120-km thickness assumed for the elastic lithosphere in the VM2 model, based upon inferences of the asymptotic thickness of oldest oceanic lithosphere (assumed to constitute a continental surrogate) by Parsons & Slater (1981), is excessive. When the recently inferred trim line observations of Ballentyne (1997) are invoked to constrain ice thickness in the Scottish Highlands, it is found that lithospheric thickness must be reduced to a value near 90 km in order to recover the reasonably good fits to the RSL data from

the west and east coasts of Scotland that had been achieved with the ICE-4G (VM2) model in which the Scottish ice sheet had been assumed to have approximately double the thickness allowed by the Ballentyne (1997) observations. Further analyses in Peltier et al. (2002) showed that this reduction in lithospheric thickness did not significantly impact the deep viscosity structure in the VM2 model. This new inference of lithospheric thickness is significantly greater than had been inferred earlier by Lambeck (1993, 1995, 1998) on the basis of analysis of data from the same region, whose work led to a preferred lithospheric thickness of 65 km. As commented in Peltier et al. (2002), it appears that the much reduced lithospheric thickness inferred by Lambeck was due to the fact that the ^{14}C dated RSL histories to which his model was fit were not converted to the calendar year timescale on which the theoretical model makes predictions. Lambeck et al. (1996, 1998) also claimed that the GIA data from the British Isles required a very sharp increase in viscosity across the 660-km seismic discontinuity from a value of approximately 0.4×10^{21} Pa s to a value of approximately 10^{22} Pa s. Although the former value for the upper mantle and transition zone is in accord with that in the VM2 model, the latter is greater by a very significant factor of five. As demonstrated in Peltier et al. (2002), however, the predictions of the VM2 model, modified solely by a reduction of lithospheric thickness from 120 km to 90 km, fits all of the GIA data from the British Isles extremely well. Although these data may allow a much higher viscosity in the lower mantle than that in VM2, they do not constrain it at all because the Scottish ice sheet is of such small horizontal scale that the response to its removal is insensitive to the viscosity structure at such extreme depth. In order to obtain significant constraints on the viscosity below a depth of 660 km, one must employ GIA data that pertain to the response of an ice sheet of largest possible horizontal scale, the sole candidate for which is the Laurentide ice sheet that covered all of Canada at LGM. That the viscosity of the upper part of the lower mantle in the VM2 model is in fact an approximate upper bound on the creep resistance in this region has been established through reanalysis of the relaxation times characteristic of the glacial rebound process at North American sites reported in Dyke & Peltier (2000). As demonstrated in Peltier (2002c), these most accurately inferred relaxation times are everywhere lower than those predicted by the ICE-4G (VM2) model.

Although support for the high lower mantle viscosity model of Lambeck and colleagues has also been claimed on the basis of model fits to RSL data from the Western Mediterranean Basin (Lambeck & Bard 2000), more recent analysis of the same data have suggested that this inference is also incorrect. The feature of the RSL data from this region, which has been construed to be diagnostic of the contrast in viscosity across the 660-km seismic discontinuity, is related to the nonexistence of a mid-Holocene highstand of the sea at sites along the south coast of France and proximate Spain. Morehange et al. (2001) have commented that an early prediction of the RSL record for the ancient harbor of Marseilles based upon the VM2 model appeared to predict the existence of such a highstand whereas none was observed. The high-viscosity contrast model of Lambeck & Bard (2000) predicts

no such highstand, suggesting that this may be the preferred model. Figure 6, however, from Peltier et al. (2003), demonstrates this conclusion to be incorrect. This figure shows predictions of the RSL history at the sites La Ciotat (France), Port Cros Is. (France), N. Corsica (France), and W. Corsica (France) in panels *a*, *b*, *c*, *d*, respectively, for the ICE-4G (VM2) model and for three variants upon it produced by successively increasing the viscosity in the entire lower mantle to 2.5, 3.5, and finally 4.5×10^{21} Pa s. Inspection shows that the highest viscosity contrast model fits the data reasonably well (although this increase in lower-mantle viscosity is rejected by the data from the two Corsican sites), whereas the pure VM2 model predicts the presence of the mid-Holocene highstand at sites along the south coast of France that is not observed, thereby tending to reinforce the validity of the Lambeck & Bard (2000) preference for a high-contrast model, although one in which the contrast is considerably reduced from their preferred value. The physical effect that is occurring in these calculations is that first noted in Peltier (1986) in connection with his analysis of data from the U.S. east coast. As the contrast in viscosity across the 660-km discontinuity is increased, the width of the glacial forebulge outboard of an ice-loaded region increases. Within the region of forebulge collapse following deglaciation, no mid-Holocene highstand ever forms. Outboard of this region, however, the mid-Holocene highstand is predicted to be a qualitatively significant feature of RSL history. Because the results of the RSL analyses shown on Figure 6 are based upon the form of the SLE given in Equation 1, which neglects the influence of time dependence of the ocean function $C(\theta, \lambda, t)$, assumes that isostatic equilibrium obtains at LGM, and neglects the influence of rotational feedback, we should be concerned that the neglect of these subtle effects could prejudice the quality of the mantle viscosity inference based upon the western Mediterranean data.

That such concern is fully warranted is demonstrated in panels *e*, *f*, *g*, and *h* of Figure 6 in which we compare the predicted RLS histories for the same set of Western Mediterranean Basin sites as in panels *a–d*. For the purpose of these intercomparisons, I have kept the viscosity structure fixed, in all but one of the models for which results are shown, to that of VM2 and simply added each of these subtle effects one at a time, first by introducing a specific model of the 100-kyr cycle of loading and unloading (prehistory), so that the assumption of isostatic equilibrium at LGM is unnecessary, next by also including the influence of rotational feedback (rotation), and finally by adding the influence of the time dependence of the coastline (Shelf effect, see Peltier & Drummond 2002). Inspection of the results of this set of analyses demonstrates that when all three subtle influences are included in the calculation, no significant increase in viscosity across the 660-km discontinuity is required to remove the mid-Holocene highstand that is otherwise predicted to exist at sites along the south coast of France. A very slight increase to approximately 3×10^{21} Pa s appears to give the best fit to all of these observations. This once more confirms the essential validity of the ICE-4G (VM2) model insofar as the VM2 viscosity structure is concerned. This last set of intercomparisons also suggests that it is primarily due to the incorporation of the influence of rotational

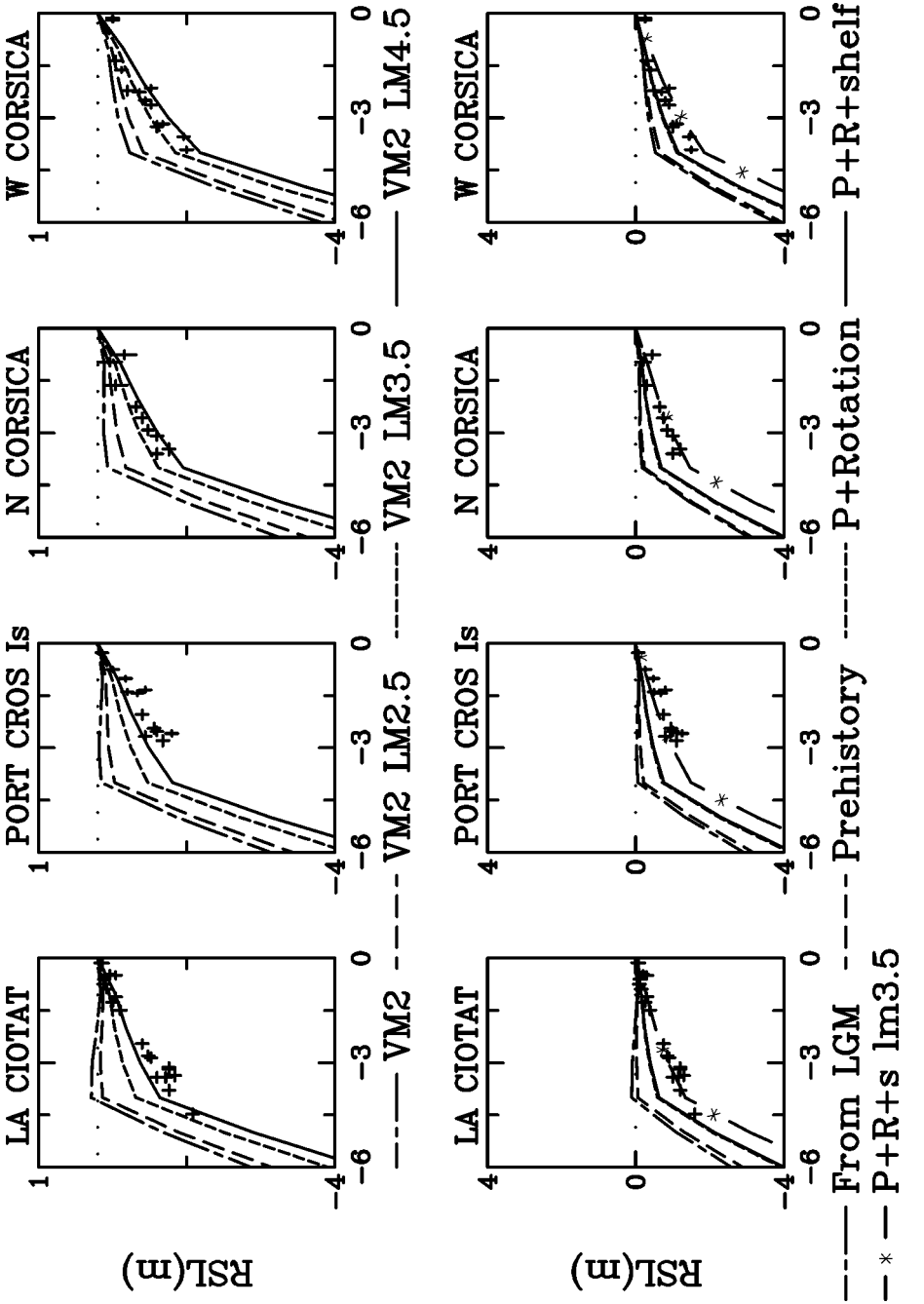

feedback, recently discussed at length in Peltier (2002c), that the ICE-4G (VM2) model is able to reconcile these data so nicely. At these locations, neither the shelf effect nor the influence of prehistory appears to be especially significant.

The accuracy of the methodology that has been developed to describe the influence of the exposure and inundation of continental shelves that occurs as continental ice sheets grow and decay has also been subjected to significant further testing in Peltier (2002a,b,c) and Peltier & Drummond (2002) by focusing upon the intercomparisons of theory and observations at sites located along the southeast coast of the South American continent in Argentinian Patagonia and on the Sunda Shelf in Indonesia. A new set of RSL data presented in Rostami et al. (2000) revealed the presence of a mid-Holocene highstand of sea level along the coast of Patagonia that reaches 5–6 m above present sea level, apparently the largest amplitude of this feature of the postglacial sea level record found anywhere in the world. Furthermore, the continental shelf outboard of this region is one of the broadest globally, much of which was fully exposed at LGM and therefore constitutes a region in which the influence of the shelf effect should be especially important. An initial analysis of the data from this region emphasizing the influence of the shelf effect was reported in Peltier & Drummond (2002) and extended in Peltier (2002c) to include the impact of the same three subtle effects discussed in regard to the Western Mediterranean data. The results of this sequence of analyses are shown in Figure 7 for Argentinian sites in the same format as for Figure 6. In this region, the influence of rotational feedback is shown to be as important as is the

Figure 6 Intercomparisons of observed and predicted Holocene RSL histories at four sites in the Western Mediterranean Basin, two from the south coast of France (La Ciotat, Port Cros) and two from the Island of Corsica. The first set of intercomparisons for these sites (*top row*) illustrates the sensitivity to lower-mantle viscosity at each site in models that are variations on the basic VM2 model of Figure 1. Note the VM2 itself predicts the existence of a mid-Holocene sea-level highstand at both La Ciotat and Port Cros, a feature that is not observed. Increasing the viscosity in the entire lower mantle of VM2 removes this feature and delivers a good fit to the observations at these two sites for lower-mantle viscosity of 4.5×10^{21} Pa s. At N. Corsica and W. Corsica, however, the data prefer a lower-mantle viscosity of 3.5×10^{21} Pa s, the higher value of 4.5×10^{21} Pa s being excessive. In the lower row of intercomparisons, the viscosity model is first fixed to MV2 and the influences of glacial prehistory, rotational feedback, and the shelf effect are added successively. The shelf effect and prehistory are found to be small influences at these locations, but rotational feedback is sufficient to allow the VM2 model to fit the data from W. Corsica extremely well without the need for any increase in viscosity. At La Ciotat, Port Cros, and N. Corsica, however, a small increase in lower-mantle viscosity above that in VM2 is needed to fit these data when the deglaciation history is fixed to that of ICE-4G. An increase to 3×10^{21} Pa s is found to deliver an excellent fit to all of the data, a change that constitutes a very minor variation upon the VM2 model.

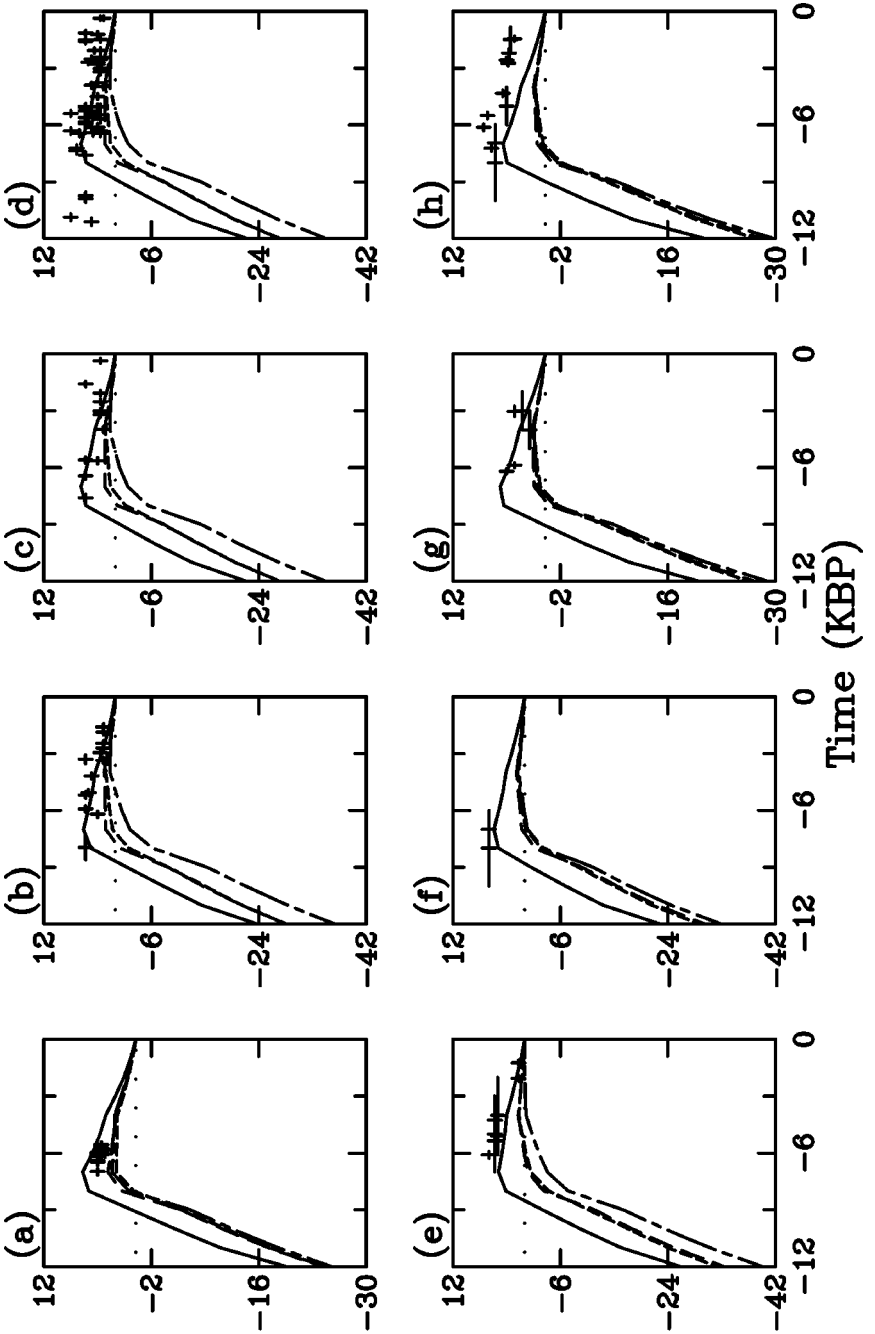

influence of the broad shelf effect, in fact, so important that in the absence of this influence the extremely large amplitude of the observed mid-Holocene highstand of sea level along this coast would remain unexplained. To fully account for the regional differences between RSL histories at sites in the far field of the ice sheets, careful attention must be paid to each of the three subtle effects upon which we have focused in connection with the discussion of Western Mediterranean and southeast South American data.

The reason why the impact of rotational feedback proves to be such an important influence in the latter region is made clear on the basis of Figure 8 on which I show ICE-4G (VM2) model predictions at global scale of the present-day rate of RSL rise. Panels *a* and *b* of Figure 8 show this prediction including (*a*) and excluding (*b*), the influence of rotational feedback. Panel *c* shows the difference in these fields, which is observed to have the form of a spherical harmonic of degree 2 and order 1. Inspection of Equations 7c and 7d shows that this form of the rotational feedback effect arises as a consequence of the dominant role that polar wander plays in controlling the impact on postglacial RSL of GIA-induced changes in planetary rotation. Panel *c* of Figure 8 shows that one of the four "bull's-eyes" in the degree 2 and order 1 pattern lies precisely upon the southeast tip of the South American continent, thereby explaining why the incorporation of the influence of rotational feedback upon the prediction of RSL histories in this region is so important. Panel *d* of this figure shows the ICE-4G (VM2) prediction of the time dependence of geoide height for the ICE-4G (VM2) model, a field obtained by adding to the field in Panel *a* the prediction of the time rate of change of the local radius of Earth calculated using Equation 8a. This is the signal that the Gravity Recovery and Climate Experiment (GRACE) satellite observes, and this is further discussed below.

Based upon the analyses discussed in this subsection, it would appear that there is no basis upon which one may argue that the VM2 radial viscoelastic structure component of the ICE-4G (VM2) model is significantly in error if proper allowance is made for the adjustment to the viscosity in the deepest lower mantle

Figure 7 Intercomparisons of observed and predicted Holocene RSL histories at eight sites along the southeast coast of the South American continent for the same set of variations upon the solution of the SLE for the ICE-4G (VM2) model described in the bottom row of Figure 6, with the different line types showing the results obtained for similar variations upon the computational procedure. Here, however, the only curve that includes the influence of rotational feedback is the solid curve. The individual locations are a subset of those for which data were assembled in Rostami et al. (2000), namely (*a*) Gualeguay, (*b*) B. Samborombon, (*c*) Pedro Luro, (*d*) Rio Colorado, (*e*) Caleta Valdes, (*f*) B. Bustamante, (*g*) Comodoro Rivadavia, (*h*) Caleta Olivia. Note that the extremely large amplitude of the mid-Holocene highstand at every one of these locations requires the influence of rotational feedback as well as the shelf effect so that the theory fits the observations. The quality of the fit achieved by the ICE-4G (VM2) model at all eight locations is excellent.

that would be required to accommodate modern-day polar ice-sheet melting and/or the presence of a low viscosity zone coincident with the seismic D″ layer and if a slight reduction of the thickness of the surface lithosphere is introduced so as to accommodate the uplift data from Scotland. Although lateral heterogeneity of the viscoelastic structure must exist on a priori grounds, the data currently available seem not to require it. As I demonstrate below, however, the ICE-4G deglaciation history component of the ICE-4G (VM2) model is not nearly so secure as is the VM2 model of the radial viscoelastic structure.

The ICE-4G Model of Würm-Wisconsin-Devensian Deglaciation History: Global and Regional Flaws

To illustrate the flaws that have recently been revealed in the ICE-4G model of deglaciation as well as its more positive aspects, I begin by drawing attention to a primary flaw. This critical flaw concerns the recognition that any successful model of the last deglaciation event of the current ice age must satisfy the available global constraints upon the net amount of water that was added to the oceans across the glacial-interglacial transition. Until recently, the sole constraint available upon the net volume of continental ice that melted during the transition from marine oxygen isotope stage 2 (MOIS 2, LGM) to MOIS 1 (the Holocene) was that provided by the coral-based data of Fairbanks (1989) on the U/Th-based timescale of Bard et al. (1990) from the island of Barbados in the Caribbean Sea off the coast of Venezuela. Very recently, however, further information has become available from the Sunda Shelf of Indonesia (Hanebuth et al. 2000) and from the J. Bonaparte Gulf of northern Australia (Yokoyama et al. 2000). Figure 9 shows the fit of the ICE-4G (VM2) model to the data from the Barbados, Sunda Shelf, and J. Bonaparte Gulf regions for the same sequence of "flavors" of the solution of the SLE as were employed in constructing the previously discussed solutions for the Mediterranean and South American sites. Inspection of these results serves to illustrate a number of important characteristics of the ICE-4G component of the ICE-4G (VM2) model.

Considering first the fit to the data at Barbados, it is clear that although neither the shelf effect nor the influence of prehistory have a significant impact at this location, there is a small impact of several meters owing to the action of rotational feedback, an impact that primarily affects the model prediction for the first few thousand years following the onset of deglaciation. Second, it is clear that the coral-based constraints upon the relative level of the sea near LGM are extremely loose as they are based upon the Porites species of coral (note the long error bars) rather than upon Acropora Palmata, a species of coral whose habitat is normally within 5 m of actual sea level in this region. The ICE-4G (VM2) model, according to this intercomparison, provides a reasonable fit to the important Barbados constraint but must be considered a minimum volume model of Würm-Wisconsin-Devensian deglaciation. Inspection of the predictions for the Sunda Shelf location, however, suggests that this minimum ice volume model may be unacceptable. At the Sunda

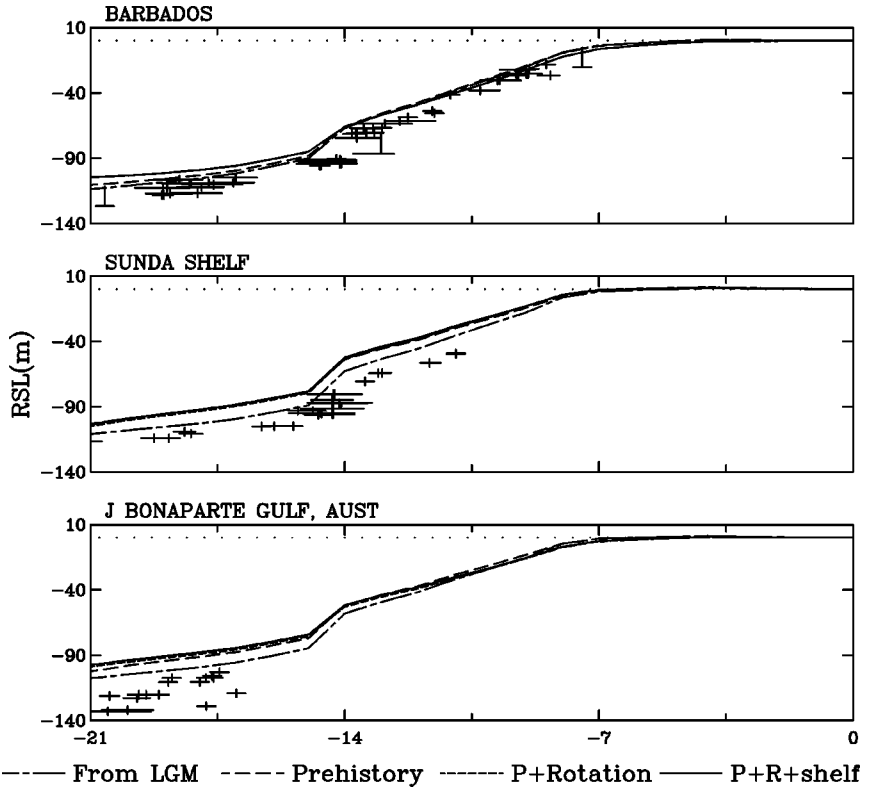

Figure 9 Intercomparisons of the observed and predicted late glacial and Holocene RSL histories at the Barbados, Sunda Shelf, and J. Bonaparte Gulf locations for the same four variants upon the analysis procedure employed in Figures 6 and 7, with the different variations described by the same line types Although the Barbados observations are only marginally misfit with the version of ICE-4G that incorporates a eustatic rise of 113.5 m, the data from the Sunda Shelf and J. Bonapart Gulf are misfit to an entirely unacceptable degree, as first pointed out in Peltier (2002a,b). The misfit in the latter two locations is such as to imply that the net eustatic rise of sea level during the last glacial-interglacial transition must have been approximately 130 m rather than the 120 m usually assumed.

Shelfs location and J. Bonaparto Gulf, although the influence of rotational feedback is essentially negligible, the regions are characterized by the presence of broad continental shelves that were largely exposed land at LGM, a consequence of which is the significant impact of the broad shelf effect at both locations. As discussed in Peltier (2002a,b) and in Peltier & Drummond (2002), the impact of this effect is to lift the predicted sea level history above that predicted by a model in which the time dependence of $C(\theta, \lambda, t)$ is included but in which no account

is taken of the restriction on the water load applied to the shelf that is required to properly conserve mass. At both the Sunda Shelf and J. Bonapart Gulf, the net effect is that the RSL observations are everywhere deeper by approximately 15 m than are the predictions of the model, implying that the ICE-4G model contains too little mass. Clearly, the magnitude of this misfit (first pointed out in Peltier 2002a,b) is highly significant, and the question naturally arises as to where on the landscape the missing mass at LGM might have resided.

Figure 10*a* shows a breakdown by region of the ice-sheet mass variations in the ICE-4G model in terms of the eustatic sea-level rise induced by the disintegration of the individual continental ice sheets. The model deglaciation history is dominated by the meltback of the North American complex, which accounts for approximately 59 m of the total of 113 m in the version of ICE-4G discussed here, a model that has been discussed at length in Peltier (2002a). This model has approximately 5 m less eustatic rise than the original ICE-4G model of Peltier (1994, 1996), a modification

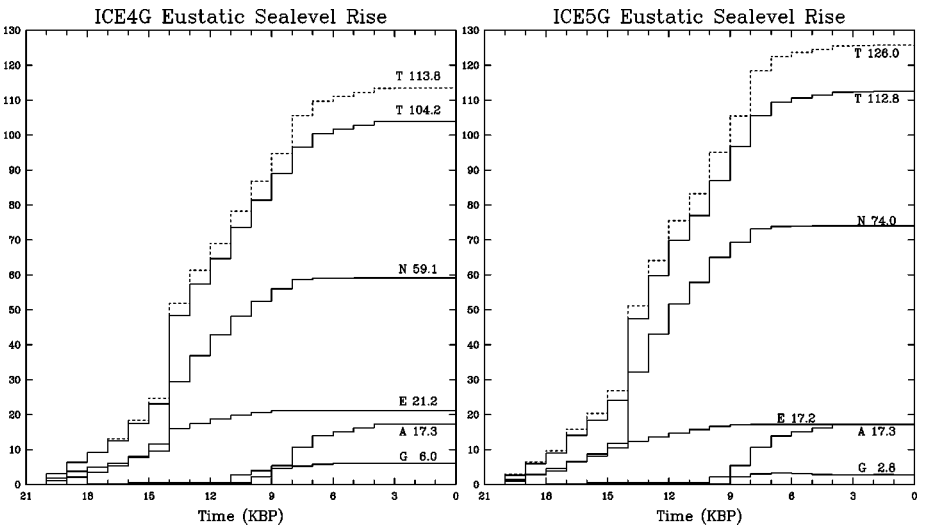

Figure 10 (*a*) Contribution of each of the individual continental ice sheets in the ICE-4G model to the net eustatic sea-level rise across the glacial interglacial transition. The segment denoted G represents the contribution from Greenland, A represents that from Antarctica, E represents that from Eurasia, and N represents the contribution from North America. T denotes the total eustatic sea-level rise delivered to the oceans owing to the sum of all contributions. The dashed segment denoted T includes the contribution to the total owing to "implicit ice" as discussed in Peltier (1998c). In this version, the ICE-4G model is therefore 113.8 m. (*b*) Same as in (*a*) but for the new ICE-5G model of the deglaciation process. Note that the contribution from the Laurentide Ice Sheet is significantly larger in ICE-5G than it was in ICE-4G, a consequence of the need to incorporate an extensive "Keewatin Dome" of ice to reconcile the new observations discussed in the text.

introduced to reduce the magnitude of the deglaciation of the Antarctic continent so as to better conform to the glaciology-based reconstructions of Huybrechts (2002) and Denton & Hughes (2002), whose analyses suggest that the loss of mass from this entire region could have caused a eustatic rise no greater than approximately 14 m, only 10% of the total eustatic rise of 120 m usually assumed (e.g., see Shackleton 2000). Also evident by inspection of Figure 10*a* is that the partial deglaciation of Antarctica is assumed to have occurred substantially later than that of the Northern Hemisphere, an assumption in the model that is also supported by the glaciological reconstructions of Huybrechts (2002) in which it is demonstrated that no significant deglaciation of Antarctica could have occurred until the Northern Hemisphere meltback had caused the sea level to rise significantly.

A further notable aspect of the ICE-4G model of global deglaciation is that it is assumed that the meltwater pulse 1a event that occurred approximately 14,000 calendar years ago, during which as much as 25 m of eustatic sea-level rise may have occurred, is sourced entirely in the Northern Hemisphere. Clarke et al. (2002) recently challenged this assumption, arguing that this dramatic event must actually have originated in the Southern Hemisphere. Their argument is based upon the claim that one may unambiguously identify the source of meltwater pulse 1a as Antarctica, based upon the difference between the predicted amplitude of MWP1A at Barbados and the Sunda Shelf, a claim that is worth revisiting here.

Figure 11 shows the relative partitioning of the Northern Hemisphere source of MWP1A in the ICE-4G model among the different geographical regions from which the meltwater is assumed to derive. Figure 12*a* shows the predicted differential amplitude of this meltwater pulse at Barbados and the Sunda Shelf for the same sequence of variants of the analysis procedure as discussed previously, but for a model in which the total mass of ice in ICE-4G has been increased so as to make up for the missing mass identified previously. This model, presented in Peltier (2002c) where it is referred to as ICE-5GP, has precisely the same MWP1A event as in ICE-4G but a net eustatic sea-level rise of approximately 125 m. Inspection of the results shown in this figure demonstrates that the maximum difference between the amplitude of MWP1A at these sites is less than 7 m, an amount which, given the error bars on the data and the significant gap in the Sunda Shelf record such that it does not explicitly record the termination of the event, is unresolvable. This fact is made clear by Figure 12*b*, which shows the MWP1A segment of the model-data intercomparison on an expanded scale for both Barbados and the Sunda Shelf. Given the ± 2.5 m error bar on the acropora palmata samples and the lack of definition at Sunda of the termination of the event, the data are unable to resolve its amplitude. Any amplitude in the range of 10 m to 25 m would appear to be allowed. There is therefore no support in these results for the argument in Clarke et al. (2002) to the effect that a significant component of MWP1A must have been sourced in Antarctica. It is nevertheless unlikely that the Southern Hemisphere ice sheets would not have responded at all to the primarily Northern Hemisphere event. What fraction of this event could have originated from this region requires further observational evidence to determine.

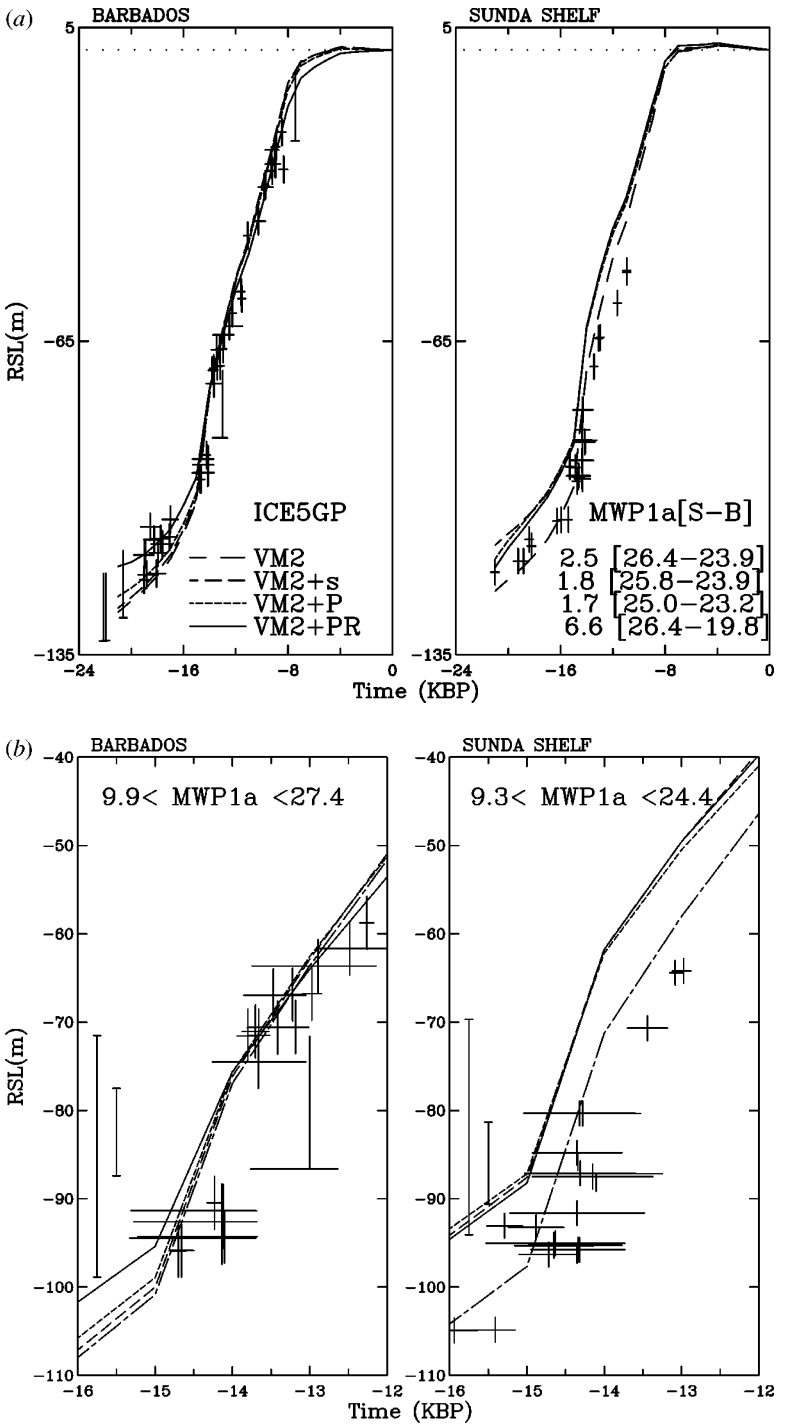

A further characteristic of the ICE-4G model (see Figure 10*a*) concerns the assumption made in constructing it: that all significant melting from both hemispheres had ceased by 4 kyr ago. The best constraint we have available on this property of the model is provided by RSL observations from island locations in the equatorial Pacific from which mid-Holocene highstand recordings are available, which show that the sea level reached the maximum elevation with respect to the land at approximately this time, subsequent to which it fell monotonically from a mid-Holocene highstand of approximately 2 m to the modern level. A detailed demonstration of the fact that the ICE-4G (VM2) model fits these observations extremely well has been provided in Peltier (2002a) and Peltier et al. (2002) as well as in Nunn & Peltier (2001) for the Fiji Islands from which an excellent data set is available. Also demonstrated in these papers is that if it is assumed that polar ice-sheet melting had continued subsequent to 4000 years ago at a rate as low as 0.5 mm year^{-1}, then these highstands would never have occurred. The only significant problem with the ICE-4G model of deglaciation would therefore appear to be the problem of missing mass suggested primarily by the recently published analyses in Peltier (2002a,b) of the Sunda Shelf and J. Bonaparte Gulf observations. Although it was suggested in Yokoyama et al. (2000) that these data required a much larger glacial-interglacial rise of eustatic sea level than the 120 m usually assumed (e.g., see Shackleton 2000), it has been pointed out in Peltier (2002b) that their argument was based upon a mathematical error. This mathematical error has been acknowledged in a recently published retraction by Yokoyama et al. (2001).

An initial indication as to where the missing mass at LGM may have been located was provided by the analysis of Argus et al. (1999) who employed a combination of VLBI and SLR observations to investigate the extent to which the radial motion and tangential motion predictions of the ICE-4G (VM2) model were consistent with these characteristics of the rebound process. Their analyses demonstrated that, with the exception of the vertical motion observation based upon the data from the space telescope at Yellowknife, the model fit the vertical motion observations extremely well. At Yellowknife, however, the observed rate of uplift was found to be more than a factor of two larger than that predicted by the ICE-4G (VM2) model. Because the ice thickness over the Keewatin Sector of the Canadian Shield on which Yellowknife is located was entirely unconstrained because no RSL data are (obviously) available from this continental interior region, it became plausible that the ice thickness over this region may have been (perhaps significantly) underestimated. This possibility was reinforced by the results of the measurements of $\dot{g}$ published by Lambert et al. (2001) at sites along a traverse from

←

Figure 12 (*a*) Differential amplitude of meltwater pulse 1a at Barbados and the Sunda Shelf for the same four variations upon the analysis procedure for the ICE-5GP model as employed in Figures 6, 7, and 9. Note that the primary cause of the differential amplitude is due to the influence of rotational feedback. (*b*) Plausible range of amplitude (in meters) for the MWP1A event at Barbados and the Sunda Shelf.

the west coast of Hudson Bay southward into Iowa. Analysis presented in Peltier (2002c; see Figure 7 in that paper) showed that the ice thickness must also have been insufficient in the region to the south and west of Hudson Bay as well as over the Keewatin Sector. The results of these analyses have therefore demonstrated that a revision of the ICE-4G component of the ICE-4G (VM2) model would be required, at least over the North American Sector. However, this is not the only region in which there existed a need for refinement of the ICE-4G reconstruction of the ice thickness history employed to describe the deglaciation process.

ICE-5G (VM2): A REFINED MODEL OF THE POST-LGM GLOBAL DEGLACIATION PROCESS

This section of the review simply summarizes the modifications to the various regional components of the ICE-4G model that have recently been implemented and explains the observational basis for these changes to the original ICE-4G reconstruction. To this end, I focus attention successively upon mainland Eurasia, Great Britain, Greenland, North America, and Antarctica.

The Eurasian Ice-Sheet Complex

The dimensions of the European ice-sheet complex that existed at LGM have been debated for decades, discussion having become polarized between two groups: those advocating the existence of extremely thick ice cover extending from Great Britain into Eastern Siberia (e.g., see Grosswald 1980, 1993, 1998) and those believing that neither the Barents and Kara Seas nor the Russian land mass was significantly glaciated at LGM (e.g., see Lavrushin 1969; Boulton 1979a,b; Troitsky et al. 1979; Matishov 1980). The CLIMAP reconstructions of Denton & Hughes (1981) for this region consisted of maximum and minimum models, both of which were strongly influenced by the "big ice" perspective of Grosswald (1980). In many respects, the ICE-4G model represented a compromise between these conflicting views [see Figure 13*a* (color insert) which shows the isostatically adjusted ice topography distribution over mainland Eurasia and the proximate shallow seas]. In this model, the Barents and Kara Seas and northern Russia were assumed to be fully glaciated, as was Fennoscandia. Notable also is the fact that no ice-bridge connection between Great Britain and Norway was assumed to exist. In the past several years, a very detailed reexamination of the glacial history of mainland Eurasia has been conducted in the context of the European Science Foundation Program entitled Quaternary Environment of the Eurasian North (QUEEN). The work undertaken in this project has dramatically increased our knowledge of the glacial history of this region as recently discussed by Svendsen et al. (1999) and more recently in papers by Mangerud et al. (2001), Mangerud et al. (2002), and Svendsen et al. (2003). This recent work has required a significant revision of the ICE-4G reconstruction, especially in the region east of Novya Zemlya. The new topography reconstruction for this region is shown in Figure 13*b*, inspection of which shows that the QUEEN results require the removal of ice cover over

most of the Kara Sea and over all of the near coastal region of northern Eurasia, including the Yamal and Kanin Penninsulas, the Pechora Sea, and the northern Siberian Plain, as well as from the islands of Severnya Zemlya. At the time the ICE-4G model was constructed, there existed no useful RSL data from this region that could be employed to test the reconstruction. Since that time, however, several excellent data sets have been produced that are valuable for this purpose, good examples of which are those presented in Zeeberg et al. (2001) from the northern part of Novaya Zemlya and from Vaygach Island in the archipelago to the south of Novaya Zemlya. Figure 14 shows RSL predictions for both the ICE-4G and ICE-5G models in comparison with these new data as well as with data from Spitzbergen and Svalbard on the northern edge of the Barents Sea. The

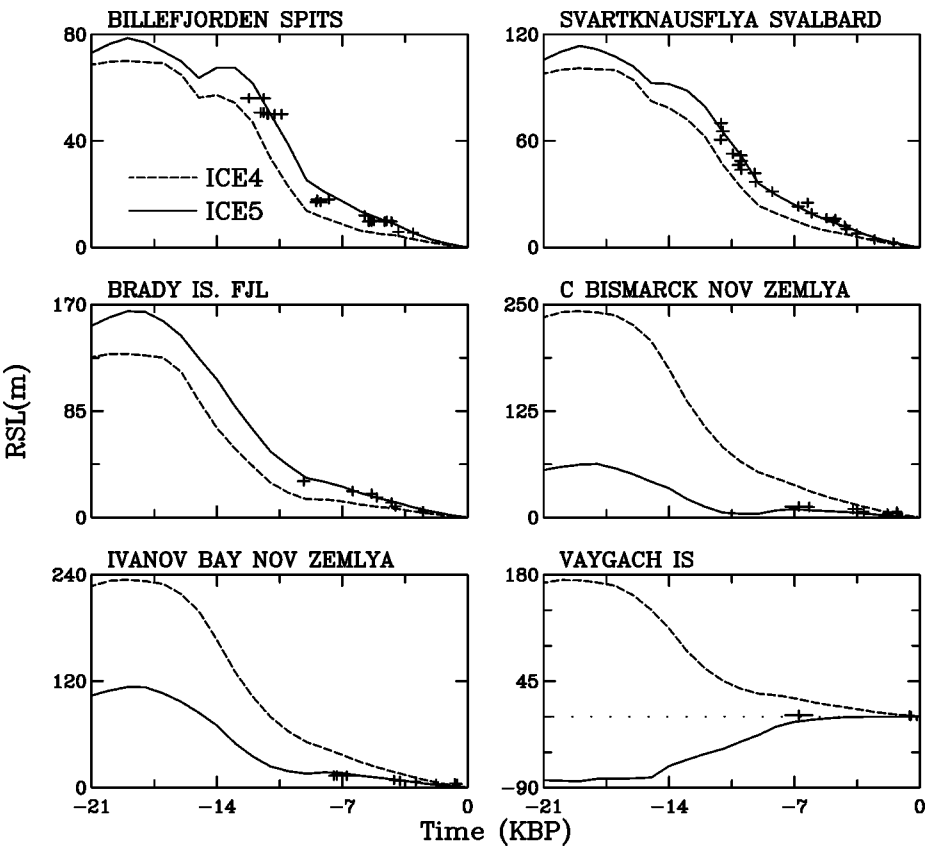

Figure 14 Intercomparisons of the observed and predicted Holocene RSL histories for six sites in the Barents and Kara Seas region of northwestern Europe illustrating the improved quality of fit obtained using the new ICE-5G model as compared to the relatively poor fits obtained using the original ICE-4G model.

most dramatic differences are those for the Novaya Zemlya and Vaygach Island sites where the new model fits the data extremely well, whereas the ICE-4G model is significantly in error.

The British Isles Ice-Sheet Complex

The British Isles component of the ICE-4G model is shown on Figure 15*a* in terms of its thickness distribution. Notable is the thickness maximum of more than 2 km over the Scottish Highlands. The very detailed recent analysis of the GIA data from the British Isles discussed in Peltier et al. (2002) has led to the marked reduction of this maximum thickness by approximately a factor of 2. The new reconstruction has since been further modified as shown in Figure 15*b* to incorporate the existence of an LGM ice-bridge between the Scottish and Norwegian ice sheets. The existence of this halo of ice surrounding the British Isles and Ireland has enabled a further reduction of ice thickness over the Scottish Highlands to be accommodated in the model, a change that has further improved the model fit to the trim line observations of Ballentyne (1997).

The Greenland Ice-Sheet at LGM

A revision of the ICE-4G reconstruction of the Greenland ice sheet has recently appeared in Tarasov & Peltier (2002). For Greenland, the problem of the inadequacy of the constraint on ice-thickness history provided by RSL data is especially acute, as the RSL data from this region are sparse and provide no significant control upon thickness variations in the core of the ice sheet where thickness is greatest. To overcome this difficulty, the analysis described in Tarasov & Peltier combines the constraint provided by the RSL data with the added constraint provided by theoretical ice mechanics. A model of the temporal variation of accumulation over the Greenland region is provided by the Greenland Ice-Sheet Project (GRIP) ice core from Summit (Dansgaard et al. 1993) over the time period from approximately 250,000 years ago until the present, and this is employed to drive a complete three-dimensional thermo-mechanical model of ice-sheet evolution (Tarasov & Peltier 1999, 2003a), configured in accord with the European Ice-Sheet Modelling Intercomparison Project (EISMINT) protocols (Payne et al. 2000). Figures 16*a,b* compare the ICE-4G and ICE-5G models of LGM Greenland ice thickness, demonstrating that the LGM thickness of central Greenland ice embodied in the ICE-4G reconstruction was excessive. Of greatest importance, however, insofar as this analysis is concerned, is that the RSL data require that the mass of the Greenland ice sheet should have increased subsequent to the mid-Holocene climatic optimum. In the absence of this regrowth of ice mass, the model is unable to reconcile the vertical motion observations from the permanent GPS receivers located at three coastal locations, observations demonstrating that the crust of Greenland is being depressed currently, a fact that is impossible to understand if only deglaciation has occurred since LGM, in which case crustal rebound would be prevalent (see Tarasov & Peltier 2002 for a detailed discussion).

The North American Ice-Sheet Complex at LGM

The problem of reconstructing the Laurentide-Innuitian-Cordilleran ice-sheet complex that covered all of Canada at LGM is even more acute than that for Greenland. Because the Greenland ice sheet was not eliminated in the deglaciation process, borehole data extracted from it can be employed to infer the variation of climate that drove its evolution through the glacial cycle. We clearly do not have this luxury for the North American ice-sheet complex, only small remnants of which continue to exist over the Queen Elizabeth Islands and Baffin Island, providing no equivalently useful record of the full glacial cycle (e.g., Koerner 1977). The ICE-4G model of the North American complex was constrained only by RSL histories from coastal sites. Although such data are in fact voluminous (over 500 distinct ^{14}C dated RSL curves are currently contained in the archive at the University of Toronto), they provide no coverage at all of the vast area of the continent that was ice covered and which lies to the west and south of Hudson Bay. The ICE-4G isostatically adjusted topography distribution for North America at LGM is shown in Figure 17*a*, which reveals a complex centered more or less over Hudson Bay with a maximum thickness of approximately 3 km. It was constrained not only by the RSL data but also by the time-dependent positions of the ice-margin catalogued in Dyke & Prest (1987). In the previous section of this review, The ICE-4G Model Of Würm-Wisconsin-Devensian Deglaciation History: Global and Regional Flaws, I have drawn attention to the fact that this model, although it fits the complete data set of RSL histories extremely well, does not fit observations of the vertical rate of motion of the crust at Yellowknife inferred on the basis of VLBI observations (Argus et al. 1999), nor does it fit the $\dot{g}$ data of Lambert et al. (2001) from sites along a traverse from the west coast of Hudson Bay at Churchill southward into the state of Iowa. Although the analyses presented in Peltier (2002c) show that both misfits may be corrected by the addition of a thick Keewatin Dome of ice over the Yellowknife region with a thick ridge of ice extending to the southeast and surrounding Hudson Bay, a structure that is exceptionally prominent in the new ICE-5G reconstruction of which a preliminary form is shown in Figure 17*b*, it is clearly of interest to determine whether, and under what conditions, an ice-sheet complex with such striking variations of topography could have been produced. In the absence of such understanding, one would be obliged to question the reasonableness of this model. Figure 18 shows the quality of the fit of the preliminary form of the ICE-5G model to the $\dot{g}$ observations of Lambert et al. (2001) using both the exact form of the theory embodied in Equation 11 as well as the approximate form embodied in Equation 13. Also shown in Figure 18 is the prediction of the ICE-4G (VM2) model, which severely underpredicts the $\dot{g}$ observations as previously discussed.

Very recently, it has proven possible to provide a detailed demonstration of the inevitableness of the development of a North American ice-sheet complex of the multidomed form implied by the requirements of these new geodetic observations. This analysis has been based upon the application of the same three-dimensional

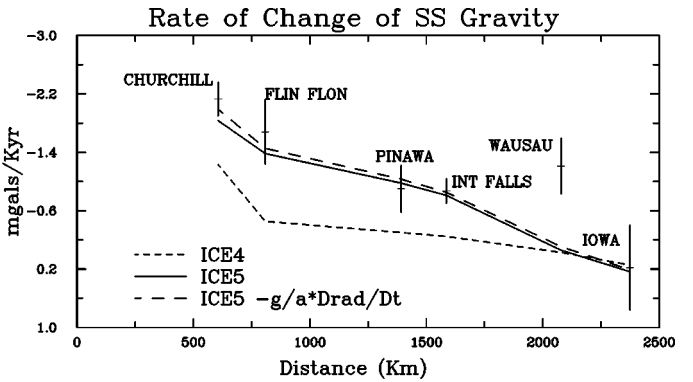

Figure 18 Intercomparison of the observations of $\dot{g}$ reported by Lambert et al. (2001) and theoretical predictions based upon the ICE-4G (VM2) and ICE-5G (VM2) models. For the latter, results are shown not only for the exact theory but also for the approximation represented by the time derivative of Equation 13.

thermomechanical ice-sheet model as that employed in Tarasov & Peltier (2002, 2003a) to describe the evolution of the Greenland ice sheet subject to the constraints provided by Holocene RSL observations. This new a priori reconstruction of the North American ice-sheet complex has been discussed in detail in Tarasov & Peltier (2003b) in which it is shown that the incorporation of the impact of subglacial sediment deformation upon the flow of the ice over the landscape is critical to the success of the model. Also of vital importance to the success of this work has been the availability of the new deglaciation chronology provided by Art Dyke of the Geological Survey of Canada (Dyke et al. 2002, 2003; Dyke 2003). The sediment cover and margin chronology maps that have been employed to constrain these new reconstructions are shown on Figures 19*a*,*b*, respectively. Inspection of the sediment cover map, from Laske & Masters (1997), shows that there exists a ring of exposed crystalline basement outboard of Hudson Bay on which we would expect the ice sheet to have been slow moving and perhaps frozen to the bed. Hudson Bay itself, however, is a basin filled by thick sediment within which it would have been possible for the ice to flow rapidly (e.g., see Payne & Dongelmans 1997). Conditions supporting the occurrence of fast flow also exist over the Canadian Prairies and throughout Southern Ontario.

A typical result for the predicted form of the Laurentide-Innuitian complex, which simultaneously fits a large set of RSL history observations as well as the Yellowknife VLBI observation and the $\dot{g}$ data of Lambert et al. derived on the basis of a large ensemble of 1200 runs of the University of Toronto Glacial Systems Model (UofT GSM), in which the parameters of the model were randomly varied through wide ranges based upon a priori understanding, is shown in Figure 20. For the purpose of these analyses, the climate forcing applied to the model of continental glaciation was once more based upon the use of the GRIP $\delta^{18}0$

record from Greenland as a basis for a bilinear interpolation between modern and LGM climates for North America derived from an average over the highest resolution general circulation model reconstructions from the PMIP ensemble (Pinot et al. 1999). Inspection of Figure 21, which shows isopacks of ice thickness superimposed upon a color-coded field of ice speed, reveals a number of important characteristics of the reconstruction. First, the model of LGM ice thickness is characterized by the presence of three distinct domes or local thickness maxima: one over the Keewatin Sector of the Shield centered near Yellowknife, a second in southeast Hudson Bay, and a third less prominent center in the Foxe Basin to the immediate west of Baffin Island. Hudson Bay itself is observed to be a local minimum of ice thickness rather than the local maximum that was characteristic of ICE-4G. Inspection of the overlay of ice speed shows that this local minimum thickness is maintained by the existence of an extremely vigorous ice stream that flows through the Hudson Strait region and that is responsible for the continuous down-draw of ice mass from the center of the Bay itself. Figure 21 shows the predicted present-day rate of radial displacement over the North American continent based upon this model of the evolution of the ice complex. Notable are the three extrema corresponding to the three primary domes of ice that dominated the ice complex at LGM, domes placed in essentially the same positions as originally suggested by the geomorphological analyses of Dyke & Prest (1987), analyses that were not considered definitive as the surface features employed to constrain their reconstruction lacked chronological control. I construe the results of the new analyses discussed herein to have firmly established the multidomed form of the Laurentide Ice Sheet at LGM.

The Antarctic Ice-Sheet Complex and Its Retreat Following LGM

The model of Antarctic deglaciation embodied in the ICE-5G (VM2) model is essentially identical to that in the modified version of the ICE-4G (VM2) model discussed in Peltier (2002a). In this model, as shown on Figure 10, the mass loss from this region is assumed to have significantly lagged Northern Hemisphere deglaciation and to have begun synchronously with the Northern Hemisphere Younger-Dryas (Y-D) event. Because this event was apparently caused by a collapse of the process of North Atlantic Deep Water (NADW) production and because a shutdown of deep water production in one hemisphere seems inevitably to lead to an increase in deep water production in the opposite hemisphere, the southern polar region would have been warmed by the Y-D cold event in the north. Combined with the rise of sea level owing to the meltback of the northern hemisphere ice sheets, this warming may have been the final trigger that induced the partial collapse of the Antarctic ice-sheet complex. Peltier (1998b) has pointed to the fact that the Antarctic component of the ICE-4G (VM2) model was assumed to be responsible for a major part of the meltwater pulse 1b revealed in the Fairbanks (1989) record from Barbados, a pulse that does indeed occur just following the

Y-D event. Minor variations upon the timing of the meltback of Antarctic ice are of course possible and several have been discussed recently in Shennan et al. (2002).

CONCLUSIONS

The new ICE-5G (VM2) reconstruction of the surface topography and land-ice distribution at LGM differs significantly from its ICE-4G (VM2) precursor. First, it contains significantly more mass of land-based ice, primarily as a consequence of the heavy ice cover that has been added outboard of Hudson Bay, ice that is required to reconcile the VLBI and $\dot{g}$ observations. The manner in which this net increase is achieved geographically, expressed in terms of the contributions from individual regions to the net rise of eustatic sea level, is illustrated in Figure 10*b*. This makes clear the dominant impact owing to the reconfiguration of the North American ice complex. Rather than accounting for a net eustatic rise of approximately 120 m as in the original ICE-4G (VM2) model of Peltier (1994, 1996), the new model ICE-5G (VM2) delivers a net eustatic rise of approximately 125 m. This is consistent with the results discussion in Peltier (2002c).

An important application of this new model of the LGM land-ice distribution is in providing the required boundary conditions on surface topography (including the land-sea distribution) and albedo that are required for the reconstruction of LGM climate using modern coupled atmosphere-ocean-sea ice models. It is expected that the influence of the thick Keewatin Dome of ice that has been inferred to exist to the west of Hudson Bay will have a strong influence on the westerly flow of air over the continent by deflecting the midlatitude jet stream southward and thereby repositioning the storm track within which precipitation is concentrated. The magnitude of this effect is currently under investigation and will be reported upon elsewhere.

An equally important application of the new model, however, will be in the analysis of the data that will soon be forthcoming from the recently launched GRACE satellite system. This dual-satellite configuration in which the separation of the two fliers is continuously monitored using a microwave link, will deliver a map of the time dependence of the gravity field of the planet that is accurate to a high degree and order in a conventional Stokes coefficient expansion. Because one of the most important contributors to the secular component of such time dependence is that due to the glacial isostatic adjustment process, it is expected that the influence this process will have to be removed from the observed secular variation of the field to more clearly observe the influence owing to modern climate change. The secular climate change–related residual is expected to be dominated by those processes associated with the ongoing rise of global sea level, including the melting of small ice sheets and glaciers, the steric effect of thermal expansion of the oceans, and perhaps also by the melting of one or both of the existing great polar ice sheets. We might, therefore, view the global model of the GIA process as defining a filter to be applied to the GRACE data. Figure 22 illustrates the difference

in the form of this filter between that defined by the previous ICE-4G (VM2) model and that defined by the new ICE-5G (VM2) model that has been under discussion herein. Although the general form of the GIA filter remains the same, the difference between the predictions of the time rate of change of geoide height for the two models is highly significant, especially over the North American continent and Greenland where the changes to the model have been especially important. The process of fully exploiting the GRACE observations will of course require, and enable, further refinement of the ICE-5G (VM2) model, both in regard to its mantle viscosity component and its deglaciation history component. Given the quality of the data set that we believe will be forthcoming, it is expected that the results of its analysis will be transformative of our understanding of several geodynamic and climatological processes.

The *Annual Review of Earth and Planetary Science* is online at http://earth.annualreviews.org

LITERATURE CITED

Airy GP. 1855. On the computations of the effect of the attraction of the mountain masses as disturbing the apparent astronomical latitude of stations in geodetic surveys. *Philos. Trans. R. Soc. London Ser. A* 145:101–11

Arendt AA, Echelmeyer KA, Harison WD, Lingle CS, Valentine VB. 2002. Rapid wastage of Alaska glaciers and their contribution to rising sea level. *Science* 297:382–86

Argus DF, Peltier WR, Watkins MM. 1999. Glacial isostatic adjustment observed using very long baseline interferometry and satellite laser ranging geodesy. *J. Geophys. Res.* 104:29077–93

Ballentyne CK. 1997. Periglacial trimlines in the Scottish Highlands. *Quat. Int.* 38:119–36

Bard E, Hamelin B, Fairbanks RG, Zindler A. 1990. Calibration of the ^{14}C timescale over the past 30,000 years using mass spectrometric U-Th ages from Barbados corals. *Nature* 345:405–9

Boulton GS. 1979a. Glacial history of the Spitzbergen archipelago and the problem of the Barents Sea ice sheet. *Boreas* 8:31–57

Boulton GS. 1979b. A model of Weichselian glacier variation in the North Atlantic region. *Boreas* 8:373–95

Butler S, Peltier WR. 2002. Thermal evolution of the Earth: models with time dependent layering of mantle-convection which satisfy the Urey ratio constraint. *J. Geophys. Res.* 107:ESE3-1–15

Carter WE, Robertson DS, Pyle TE, Diammante J. 1986. The application of geodetic radio interferometric surveying to the monitoring of sea level. *Geophys. J. R. Astron. Soc.* 87:3–13

Cheng MK, Eanes RJ, Shum CK, Schutz BE, Tapley BD. 1989. Temporal variations in low degree zonal harmonics from Starlette orbit analysis. *Geophys. Res. Lett.* 16:393–96

Clark JA, Farrell WE, Peltier WR. 1978. Global changes in postglacial sea level: a numerical calculation. *Quat. Res.* 9:265–87

Cox CM, Chao BF. 2002. Detection of a large mass redistribution in the terrestrial system since 1998. *Science* 297:831–33

Dahlen FA. 1976. The passive influence of the oceans upon the rotation of the Earth. *Geophys. J. R. Astron. Soc.* 46:363–406

Dansgaard W, Johnsen SJ, Clausen HB, Dahl-Jensen D, Gundestrup NS, et al. 1993. Evidence for general instability of past climate from a 250-kyr ice-core record. *Nature* 364:218–20

Denton GH, Hughes T. 1981. *The Last Great Ice Sheets*. New York: Wiley-Interscience

Denton GH, Hughes T. 2002. Reconstructing the Antarctic ice sheet at the Last Glacial Maximum. *Quat. Sci. Rev.* 21:193–202

Dickey JO, Marcus SL, de Viron Ol, Fukumori I. 2002. Recent Earth oblateness variations: unravelling climate and postglacial rebound effects. *Science* 298:1975–77

Dutton GE. 1889. On some of the greater problems of physical geology. *Bull. Philos. Soc. Wash.* 11:51–59

Dyke AS, Prest VK. 1987. Late Wisconsian and Holocene history of the Laurentide ice sheet. *Geog. Phys. Quat.* 41:237–64

Dyke AS, Peltier WR. 2000. Forms, response times and variability of relative sea level curves, glaciated North America. *Geomorphology* 32:315–33

Dyke AS, Andrews JT, Clark PU, England JH, Miller GH, et al. 2002. The Laurentide and Innuitian ice sheets during the Last Glacial Maximum. *Quat. Sci. Rev.* 21:9–31

Dyke AS, Moore A, Robertson L. 2003. *Deglaciation of North America. Thirty-two maps at 1:70000000 scale with accompanying digital chronological database and one poster (in two sheets) with full map series. Geol. Surv. Can. Tech. Rep. Open File 1574*

Dyke AS. 2003. An outline of North American deglaciation with emphasis on central and northern Canada. In *INQUA Volume of North American Glaciation*, ed. J Ehlers. In press

Dyurgerov MB, Meier MF. 2000. Twentieth century climate change: evidence from small glaciers. *Proc. Natl. Acad. Sci. USA* 97:1406–11

Dziewonski AM, Anderson DL. 1981. Preliminary reference Earth model. *Phys. Earth Planet. Int.* 25:297–356

Fairbanks RG. 1989. A 17,000-year glacio-eustatic sea level records: influence of glacial melting rates on the Younger-Dryas event and deep-ocean circulation. *Nature* 342:637–41

Faller J. 1967. Precision measurement of the acceleration of gravity. *Science* 158:60

Faller J. 1995. A new generation of absolute gravimeters. *Metrologia* 32:159–80

Faller J. 2002. Thirty years of progress in absolute gravimetry: a scientific capability implemented by technological advances. *Metrologia* 39:425–28

Faller J, Marson I. 1986. ġ—The acceleration of gravity: its measurement and its importance. *J. Phys. Earth Sci. Instr.* 9:22–32

Faller J, Vitouchkine A. 2002. Measurement results with a small cam-driven absolute gravimeter. *Metrologia* 39:429–34

Farrell WE. 1972. Deformation of the Earth by surface loads. *Rev. Geophys.* 10:761–97

Farrell WE, Clarke JA. 1976. On postglacial sea level. *Geophys. J. R. Astron. Soc.* 46:647–67

Hanebuth T, Statteger K, Grootes PM. 2000. Rapid flooding of the Sunda Shelf: a late glacial sea level record. *Science* 288:1033–35

Haskell NA. 1935. The motion of a fluid under a surface load, 1. *Physics* 6:265–69

Huybrechts P. 2002. Sea level changes at LGM from ice-dynamic reconstructions of the Greenland and Antarctic ice sheets during the glacial cycles. *Quat. Sci. Rev.* 21:203–31

Grosswald MG. 1980. Late Weichselian ice sheets of northern Eurasia. *Quat. Res.* 13:1–32

Grosswald MG. 1993. Extent and melting history of the late Weichselian ice sheet, the Barents-Kara continental margin. In *Ice in the Climate System*, ed. WR Peltier, NATO ASI Ser., pp. 1–20. Berlin: Springer-Verlag

Grosswald MG. 1998. Late Weichselian ice sheets in Arctic and Pacific Siberia. *Quat. Int.* 45/46:3–18

Johansson JM, Davis JL, Scherneck H-G, Milne GA, Vermeer M, et al. 2002. Continuous GPS measurements of postglacial adjustment in Fennoscandia, I. Geodetic Results. *J. Geophys. Res.* 107:DOI10.1029/2001JB000400

Karato S-I, Wu P. 1993. Rheology of the upper mantle: a synthesis. *Science* 260:771–75

Keay J. 2000. *The Great Arc*. London: Harper-Collins

Koerner RM. 1977. Devon Island ice cap:

core stratigraphy and paleoclimate. *Science* 196:15–18

Lambeck K. 1993. Glacial rebound of the British Isles—II. A high resolution, high precision model. *Geophys. J. Int.* 115:960–90

Lambeck K. 1995. Late Devonsian and Holocene shorelines of the British Isles and the North Sea from models of glacio-hydro-isostatic rebound. *J. Geol. Soc. London* 152:437–48

Lambeck K. 1998. On the choice of timescale in glacial rebound modelling: mantle viscosity estimates and the radiocarbon timescale. *Geophys. J. Int.* 134:647–51

Lambeck K, Bard E. 2000. Sea level change along the French Mediterranean coast for the past 30000 years. *Earth Planet Sci. Lett.* 175:203–22

Lambeck K, Johnston P, Smither P, Nakada M. 1996. Glacial rebound of the British Isles—III. Constraints on mantle viscosity. *Geophys. J. Int.* 125:340–54

Lambeck K, Smither C, Johnston P. 1998. Sea level change, glacial rebound and mantle viscosity for northern Europe. *Geophys. J. Int.* 134:102–44

Lambert A, Courtier N, Sasegawa GS, Klopping F, Winester D, et al. 2001. New constraints on Laurentide postglacial rebound from absolute gravity measurements. *Geophys. Res. Lett.* 28:2109–12

Laske G, Masters G. 1997. A global digital map of sediment thickness. *EOS Trans. Am. Geophys. Union* 78:F483

Lavrushin JA. 1969. Quaternary deposits of Spitsbergen. Pouc VIII Congr. l′INQUA, Paris. Nauka, Moskua. 1777 pp. Int. Engl. Transl., Norw. Polar Res. Inst., Oslo

Levitus S, Antonov JI, Boyer TP, Stevens C. 2000. Warming of the world ocean. *Science* 287:2225–29

Levitus S, Antonov JI, Wang J, Delworth TL, Dixon KW, Broccoli AJ. 2001. Anthropogenic warming of the Earth's climate system. *Science* 292:267–70

Mangerud J, Astakhov VI, Murray A, Svendsen JI. 2001. The chronology of a large ice-damned lake and the Barents-Kara ice sheet advances. *Global and Planet. Change* 31:321–36

Mangerud J, Astakhov V, Svendsen J-I. 2002. The extent of the Barents-Kara ice sheet during the Last Glacial Maximum. *Quat. Sci. Rev.* 21:111–19

Matishov GG. 1980. Geomorphological signs of the action of the Scandinavian, Novaya, Zemlya, and Spitsbergen ice sheets on the floor of the Barents Sea. *Oceanology* 30:440–47

McConnell RK. 1968. Viscosity of the mantle from relaxation time spectra of isostatic adjustment. *J. Geophys. Res.* 73:7089–105

Meier M. 1984. Contributions of small glaciers to global sea level. *Science* 226:1418–21

Mitrovica JX, Peltier WR. 1993. Present day secular variations in the zonal harmonics of the Earth's geopotential. *J. Geophys. Res.* 98:4509–26

Morehange C, Laborel J, Hesnard A. 2001. Changes in relative sea level during the past 5000 years in the ancient harbor of Marseilles, southern France. *Palaeogeogr. Palaeoclimatol. Palaeoecol.* 166:319–29

Munk W. 2002. Twentieth century sea level: an enigma. *PNAS* 99:6550–55

Niskanen E. 1939. On the upheaval of the land in Fennoscandia. *Ann. Acad. Sci. Fennicae AIII* 53:1–10

Payne AJ, Dongelmans PW. 1997. Self-organization in the thermomechanical flow of ice sheets. *J. Geophys. Res.* 102:12219–34

Peltier WR. 1974. The impulse response of a Maxwell Earth. *Rev. Geophys. Space Phys.* 12:649–69

Peltier WR. 1976. Glacial isostatic adjustment II. The inverse problem. *Geophys. J. R. Astron. Soc.* 46:669–706

Peltier WR. 1982. Dynamics of the ice age Earth. *Adv. Geophys.* 24:1–146

Peltier WR. 1983. Constraint on deep mantle viscosity from LAGEOS acceleration data. *Nature* 304:434–36

Peltier WR. 1985. The LAGEOS constraint on deep mantle viscosity: results from a new normal mode method for the inversion of

viscoelastic relaxation spectra. *J. Geophys. Res.* 90:9411–21
Peltier WR. 1986. Deglaciation induced vertical motion of the North American continent and transient lower mantle rheology. *J. Geophys. Res.* 91:9099–123
Peltier WR. 1994. Ice age paleotopography. *Science* 265:195–201
Peltier WR. 1996. Mantle viscosity and ice age ice sheet topography. *Science* 273:1359–64
Peltier WR. 1998a. The inverse problem for mantle viscosity. *Inverse Probl.* 14:441–78
Peltier WR. 1998b. Postglacial variations in the level of the sea: implications for climate dynamics and solid-earth geophysics. *Rev. Geophys.* 36:603–89
Peltier WR. 1998c. "Implicit ice" in the global theory of glacial isostatic adjustment. *Geophys. Res. Lett.* 25:3955–58
Peltier WR. 1999. Global sea level rise and glacial isostatic adjustment. *Global Planet. Change* 20:93–123
Peltier WR. 2002a. On eustatic sea level history: Last Glacial Maximum to Holocene. *Quat. Sci. Rev.* 21:377–96
Peltier WR. 2002b. Comments on the paper of Yokoyama et al. 2000 entitled 'Timing of the last glacial maximum from observed sea level minima.' *Quat. Sci. Rev.* 21:409–14
Peltier WR. 2002c. Global glacial isostatic adjustment: palaeogeodetic and space-geodetic tests of the ICE-4G (VM2) model. *J. Quat. Sci.* 17:491–510
Peltier WR. 2002d. Global glacial isostatic adjustment and modern instrumental records of relative sea level history. In *Sea Level Rise*, eds. BC Douglas, MS Kearney, SP Leatherman, pp. 65–95. San Diego: Academic
Peltier WR, Andrews JT. 1976. Glacial isostatic adjustment I: the forward problem. *Geophys. J. R. Astron. Soc.* 46:605–46
Peltier WR, Drummond R. 2002. A "broad shelf effect" in the global theory of postglacial relative sea level history. *Geophys. Res. Lett.* 29:10.102912001GL014273
Peltier WR, Farrell WE, Clark JA. 1978. Glacial isostasy and relative sea level: a global finite element model. *Tectonophysics* 50:81–110
Peltier WR, Jiang X. 1996. Mantle viscosity from the simultaneous inversion of multiple data sets pertaining to postglacial rebound. *Geophys. Res. Lett.* 23:503–6
Peltier WR, Morehange C, Pirazzoli P. 2003. Geodynamic implications of postglacial sea level histories in the Western Mediterranean Basin. *Earth Planet. Sci. Lett.* In press
Peltier WR, Shennan I, Drummond R, Horton B. 2002. On the postglacial isostatic adjustment of the British Isles and the shallow viscoelastic structure of the Earth. *Geophys. J. Int.* 148:443–75
Pinot S, Ramstein G, Harrison SP, Prentice IC, Guiot J, et al. 1999. Tropical paleoclimates at the Last Glacial Maximum: comparison of Paleoclimate Modelling Intercomparison Project (PMIP) simulations and paleodata. *Climate Dyn.* 15:857–74
Pratt JH. 1855. On the attraction of the Himalaya Mountains and of the elevated regions beyond upon the plumb-line in India. *Philos. Trans. R. Soc. London Ser. A* 145:53
Rostami K, Peltier WR, Mangini A. 2000. Quaternary marine terraces, sea level changes and uplift history of Patagonia, Argentina: comparisons with predictions of the ICE-4G (VM2) model of the global process of glacial isostatic adjustment. *Quat. Sci. Rev.* 19:1495–525
Shennan I, Peltier WR, Drummond R, Horton B. 2002. Local to global effects in postglacial sea level variations in the British Isles. *Quat. Sci. Rev.* 21:397–409
Shackleton NJ. 2000. The 100,000-year ice-age cycle identified and found to lag temperature, carbon-dioxide and orbital eccentricity. *Science* 289:1897–902
Stuiver M, Reimer PJ, Bard E, Beck JW, Burr JS, et al. 1998. INTCAL98 radiocarbon age calibration, 24,000—0 cal BP. *Radiocarbon* 40:1041–83
Svendsen JI, Astrakov VI, Yu D, Bolshiyanov ID, Dowdeswell JA, et al. 1999. Maximum extent of the Eurasian ice sheets in the Barents and Kara Sea reagion during the Weichselian. *Boreas* 28:234–42
Svendsen JI, Gataullin V, Mangerud J, Polyak

K. 2003. The glacial history of the Barents and Kara Sea region. In *Quaternary Glaciations—Extent and Chronology*, ed. J Ehlers, P Gibbard, Vol. 1. Amsterdam: Elsevier

Tarantola A, Valette B. 1982a. Inverse problems = quest for information. *J. Geophys.* 50:159–70

Tarantola A, Valette B. 1982b. Generalized nonlinear inverse problems solved using the least squares criterion. *Rev. Geophys.* 20:219–32

Tarasov L, Peltier WR. 1999. Impact of thermomechanical ice sheet coupling on a model of the 100 kyr ice age cycle. *J. Geophys. Res.* 104:9517–45

Tarasov L, Peltier WR. 2002. Greenland glacial history and local geodynamic consequences. *Geophys. J. Int.* 150:198–229

Tarasov L, Peltier WR. 2003a. Greenland glacial history, borehole constraints and Eemian extent. *J. Geophys. Res.* 108(B3): 2143, doi: 10.102912001JB001731

Tarasov L, Peltier WR. 2003b. A geophysically constrained large ensemble analysis of the deglaciation history of the North American ice sheet complex. *Quat. Sci. Rev.* In press

Tushingham AM, Peltier WR. 1991. ICE-3G: a new global model of late Pleistocene deglaciation based upon geophysical predictions of post-glacial relative sea level change. *J. Geophys. Res.* 96:4497–523

Tushingham AM, Peltier WR. 1992. Validation of the ICE-3G model of Würm-Wisconsin deglaciation using a global data base of relative sea level histories. *J. Geophys. Res.* 97:3285–304

Troitsky L, Panning J-M, Hütt G, Rajamae R. 1979. Pleistocene glaciation chronology of Spitsbergen. *Boreas* 8:401–7

Vincente RO, Yumi S. 1969. Co-ordinates of the pole (1899–1968) returned to the conventional international origin. *Publ. Int. Latit. Obs. Mizusawa* 7:41–50

Vincente RO, Yumi S. 1970. Revised values (1941–1961) of the co-ordinates of the pole referred to the CIO. *Publ. Int. Latit. Obs. Mizusawa* 7:109–12

Wu P, Peltier WR. 1982. Viscous gravitational relaxation. *Geophys. J. R. Astron. Soc.* 70:435–85

Wu P, Peltier WR. 1984. Pleistocene deglaciation and the Earth's rotation: a new analysis. *Geophys. J. R. Astron. Soc.* 76:202–42

Yoder CF, Williams JG, Dickey JO, Schutz BE, Eanes RJ, Tapley BD. 1983. Secular variation of the Earth's gravitational harmonic J_2 coefficient from LAGEOS and non-tidal acceleration of Earth rotation. *Nature* 303:757–62

Yokoyama Y, Lambeck K, de Dekhar P, Johnston P, Fifield LK. 2000. Timing of the last glacial maximum from observed sea-level minima. *Nature* 406:713–16. Correction 2001. *Nature* 412:99

Zeeberg J, Lubinski DJ, Forman SL. 2001. Holocene relative sea level history of Novya Zemlya, Russia, and implications for late Weichselian ice-sheet loading. *Quat. Res.* 56:218–30

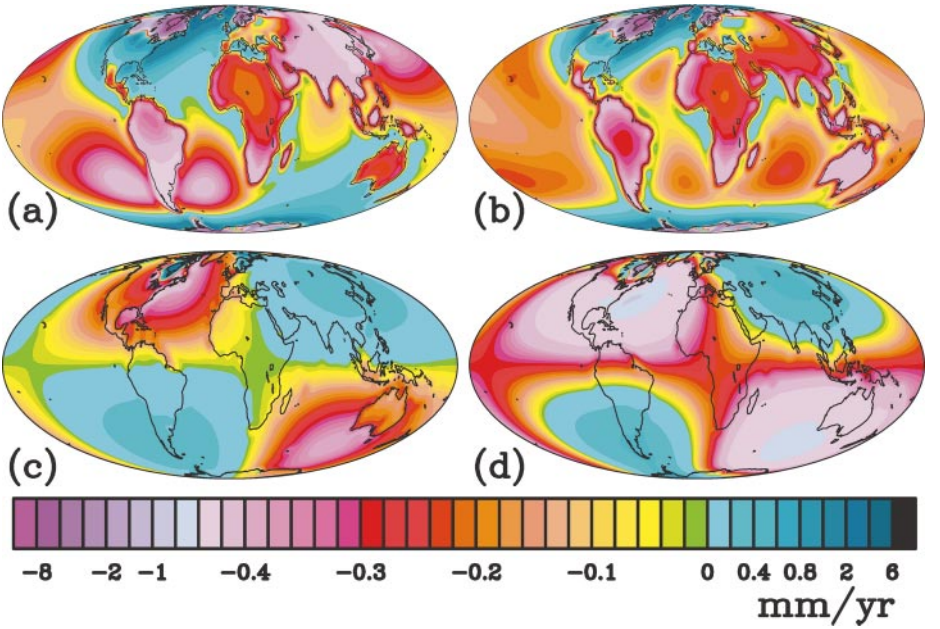

Figure 8 ICE-4G (VM2) model prediction of (*a*) the present-day rate of sea-level rise relative to the deforming surface of the solid Earth, including the influence of rotational feedback; (*b*) same as (*a*) but excluding the influence of rotational feedback; (*c*) the difference between (*a*) and (*b*) illustrating the spherical harmonic degree 2 and order 1 pattern that dominates the influence owing to rotational feedback on account of the control exerted by the polar wander effect; (*d*) the present-day geoide height time dependence predicted by the ICE-4G (VM2) model, obtained by adding to the field in (*a*) the prediction of the time rate of change of radial displacement with respect to the center of mass of the planet.

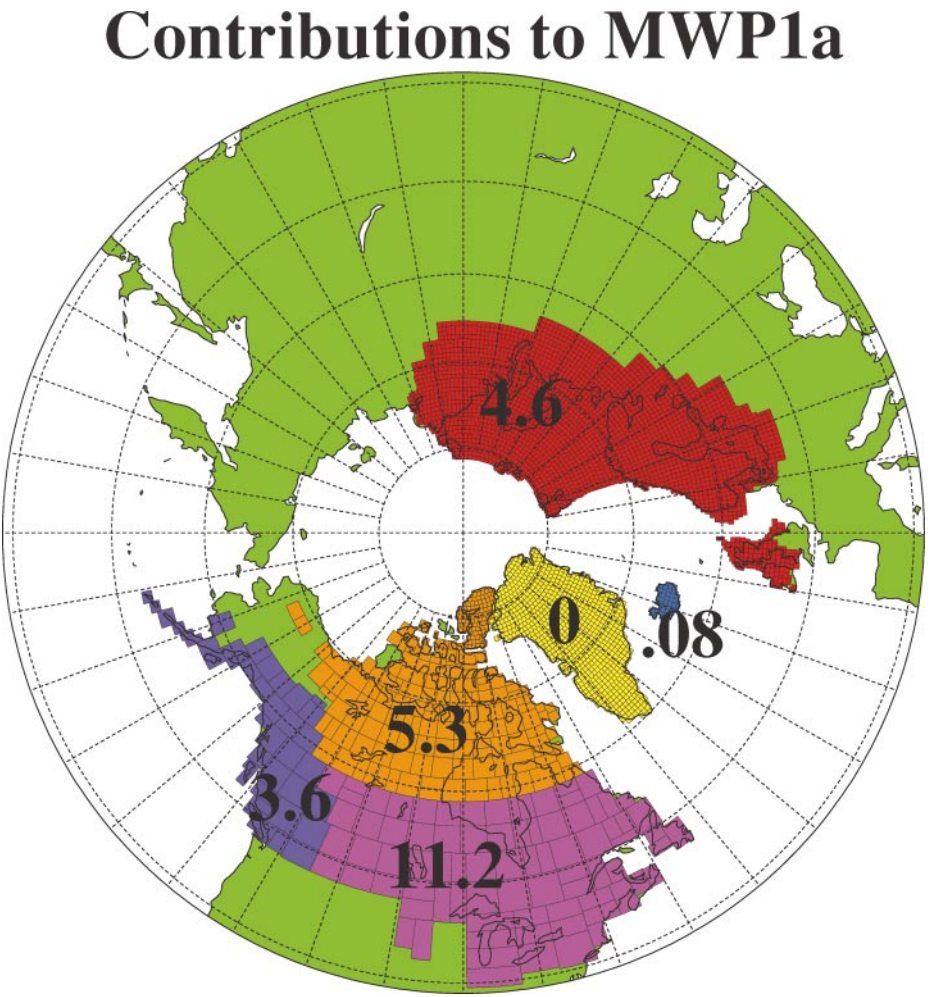

Figure 11 Magnitude in meters of eustatic sea-level rise contributed to the meltwater pulse 1a event from individual geographical regions in the ICE-4G model of deglaciation.

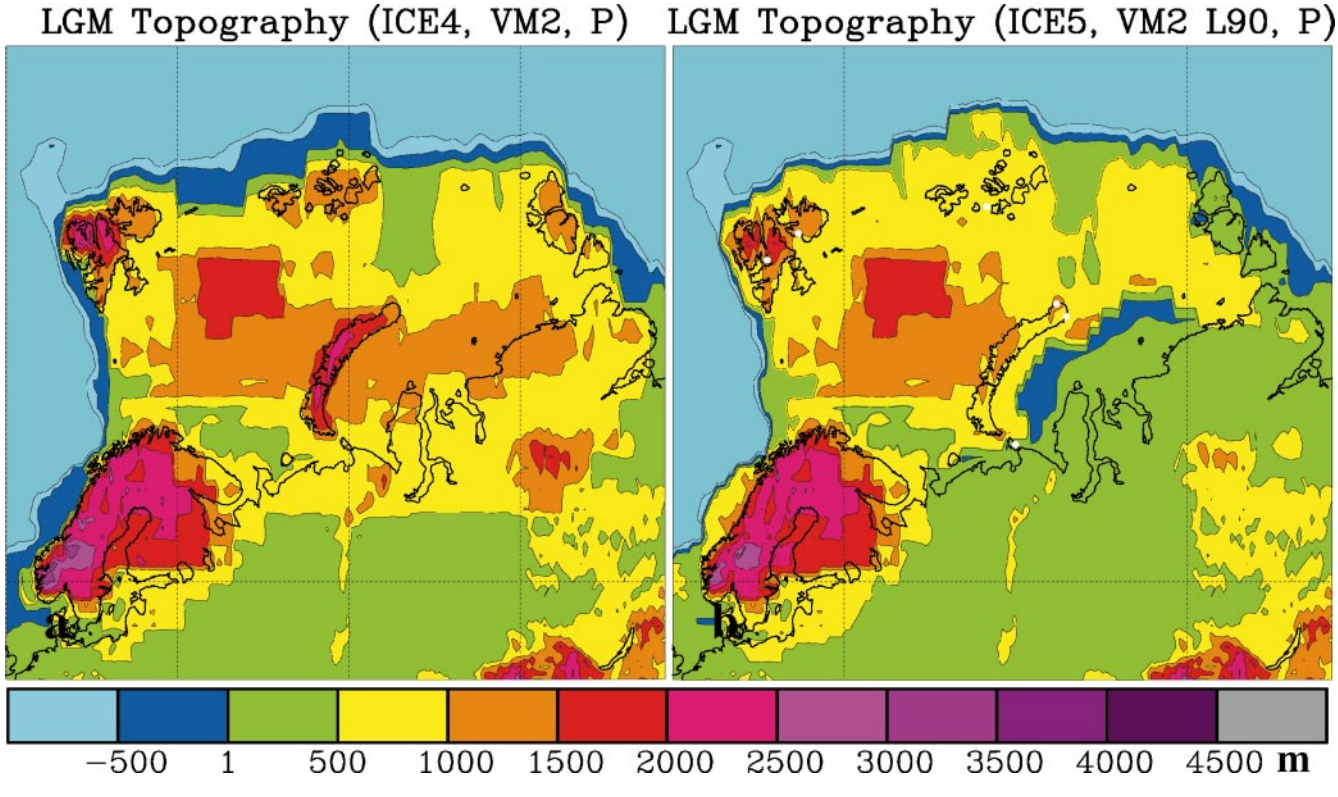

Figure 13 (*a*) The isostatically adjusted topography over mainland Eurasia according to the ICE-4G (VM2) model. (*b*) Same as (*a*) but for the new ICE-5G (VM2) model.

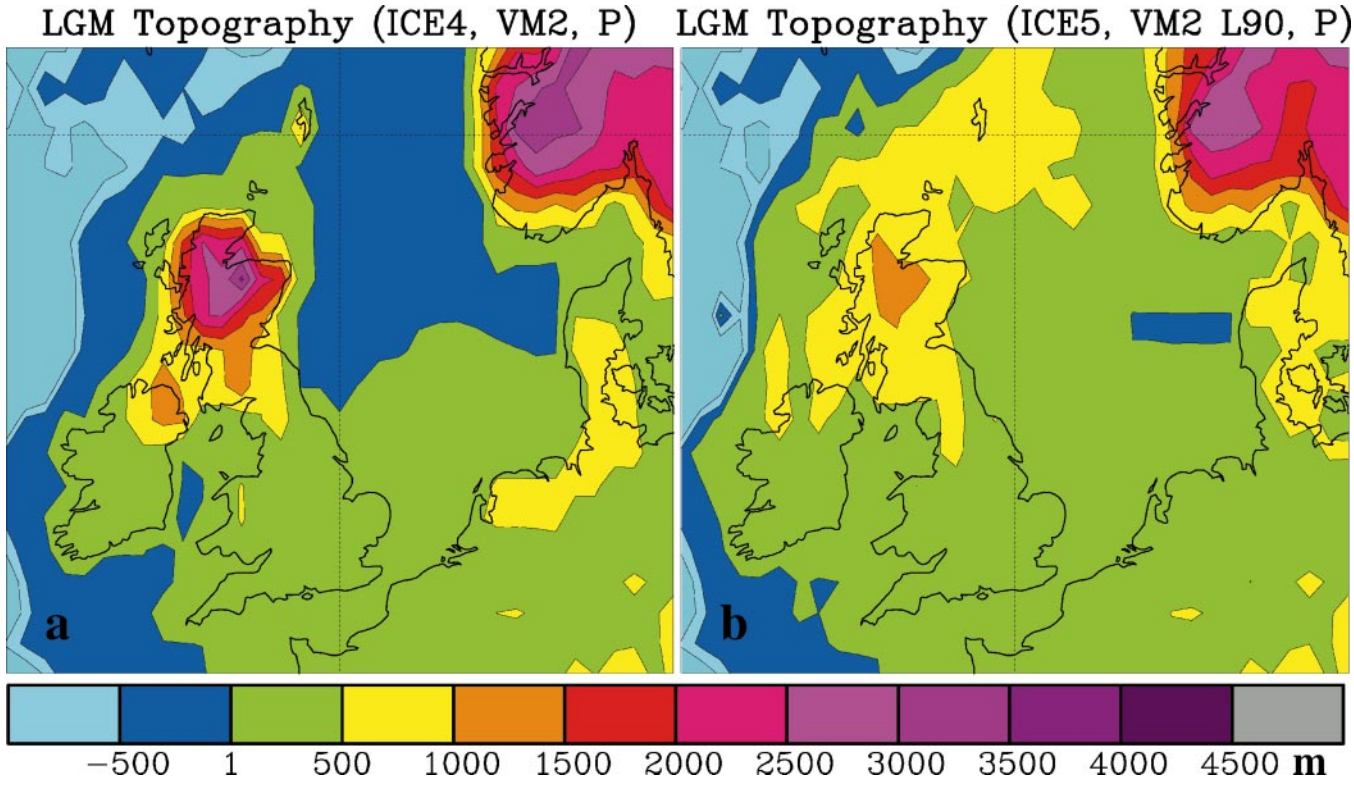

Figure 15 (*a*) Isostatically adjusted topography for the ICE-4G model over the British Isles. (*b*) Same as (*a*) but for the ICE-5G model.

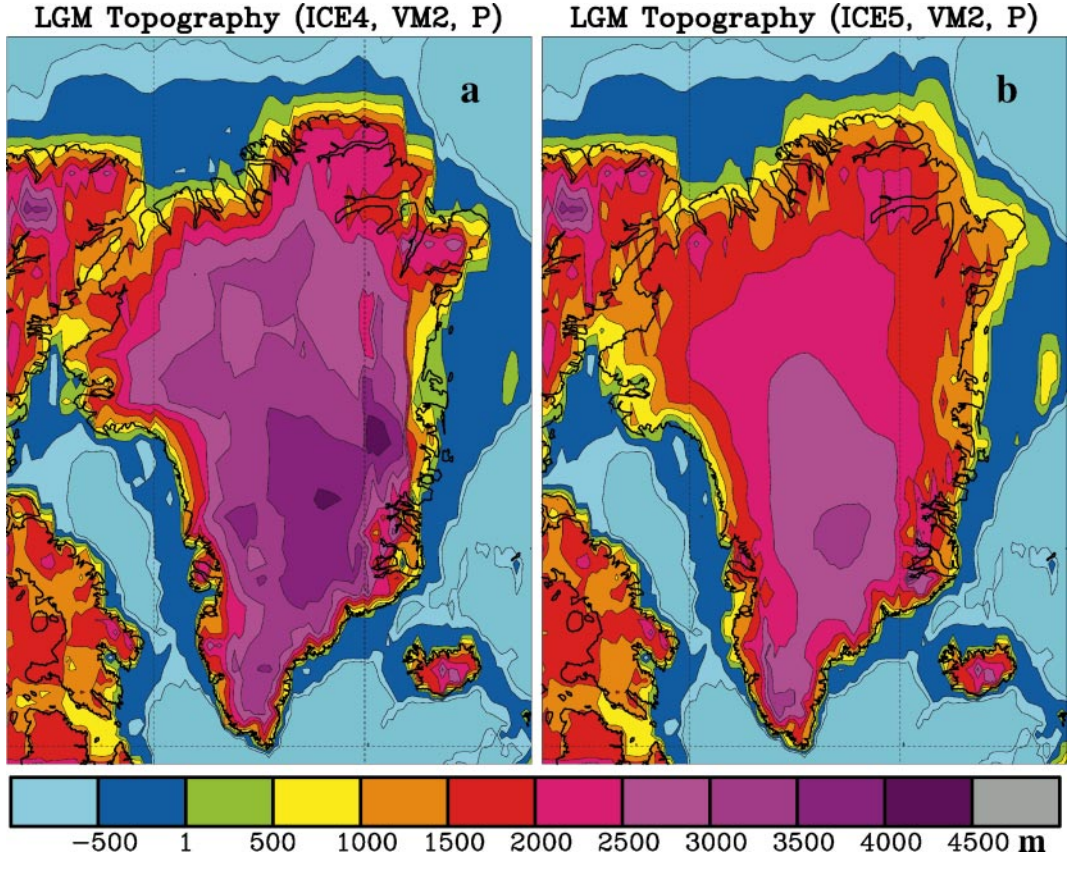

Figure 16 (*a*) Isostatically adjusted topography for the ICE-4G model over Greenland. (*b*) Same as (*a*) but for the ICE-5G model.

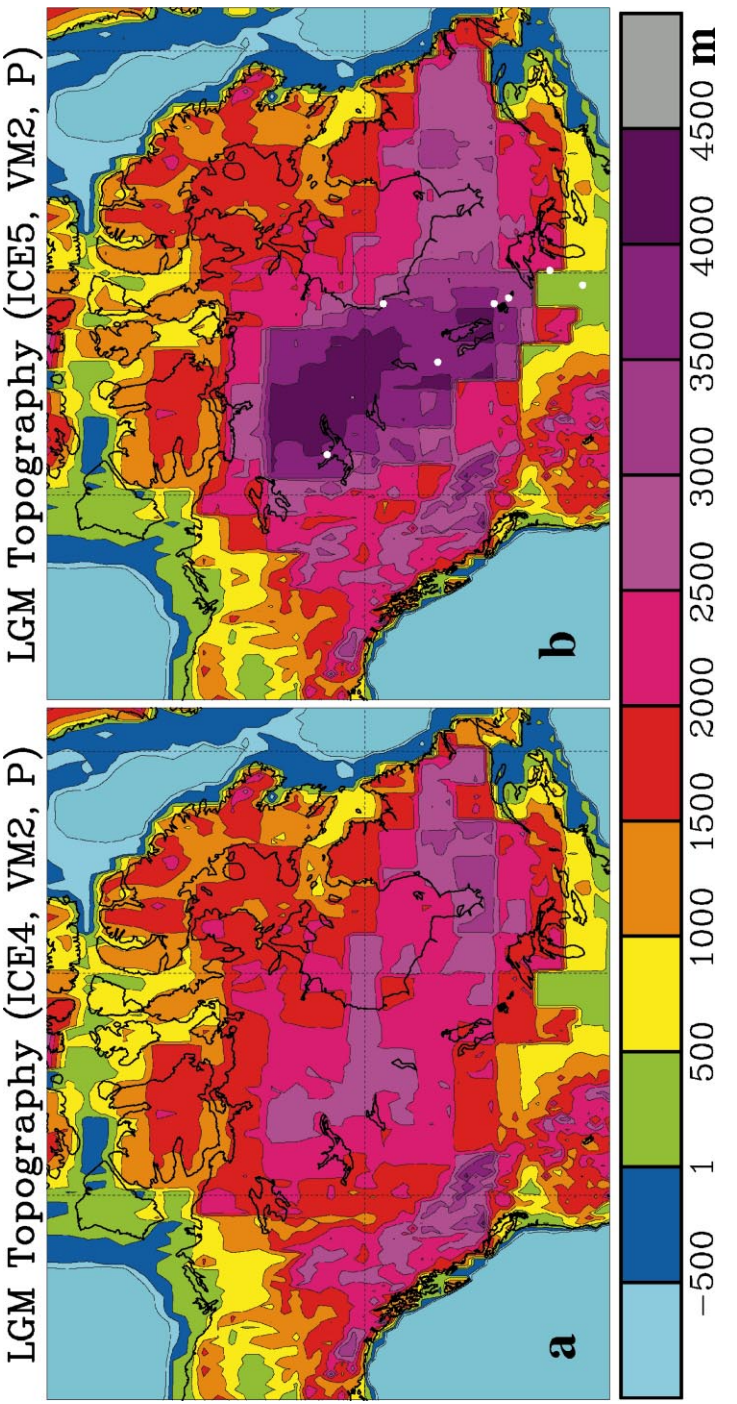

Figure 17 (*a*) Isostatically adjusted topography for the ICE-4G model over North America. (*b*) Same as (*a*) but for the ICE-5G model.

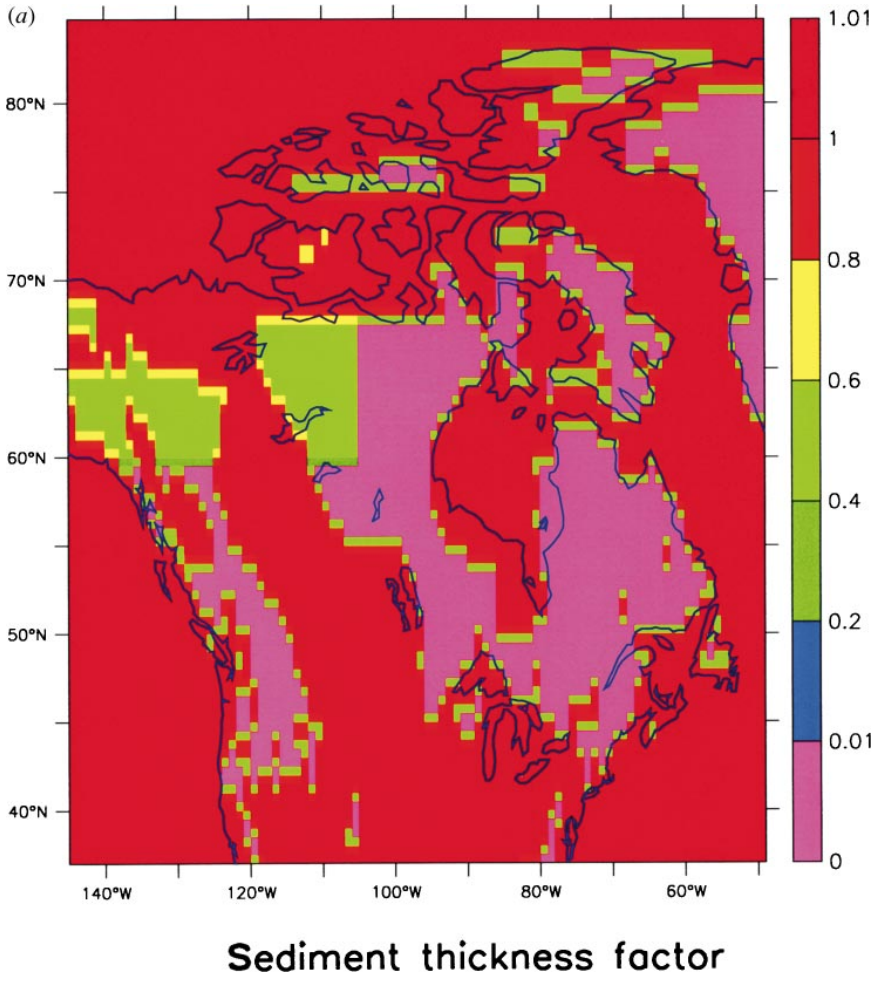

Figure 19 (*a*) Sediment thickness map for the North American continent employed to compute the impact of sediment deformation upon the velocity of ice-sheet flow (from Laske & Masters 1993; the numerical values corresponding to the color bar are based upon a division of actual sediment thickness by 20 m). (*b*) Example Laurentide ice sheet margin positions from the new high-resolution margin chronology of Dyke (2002a,b).

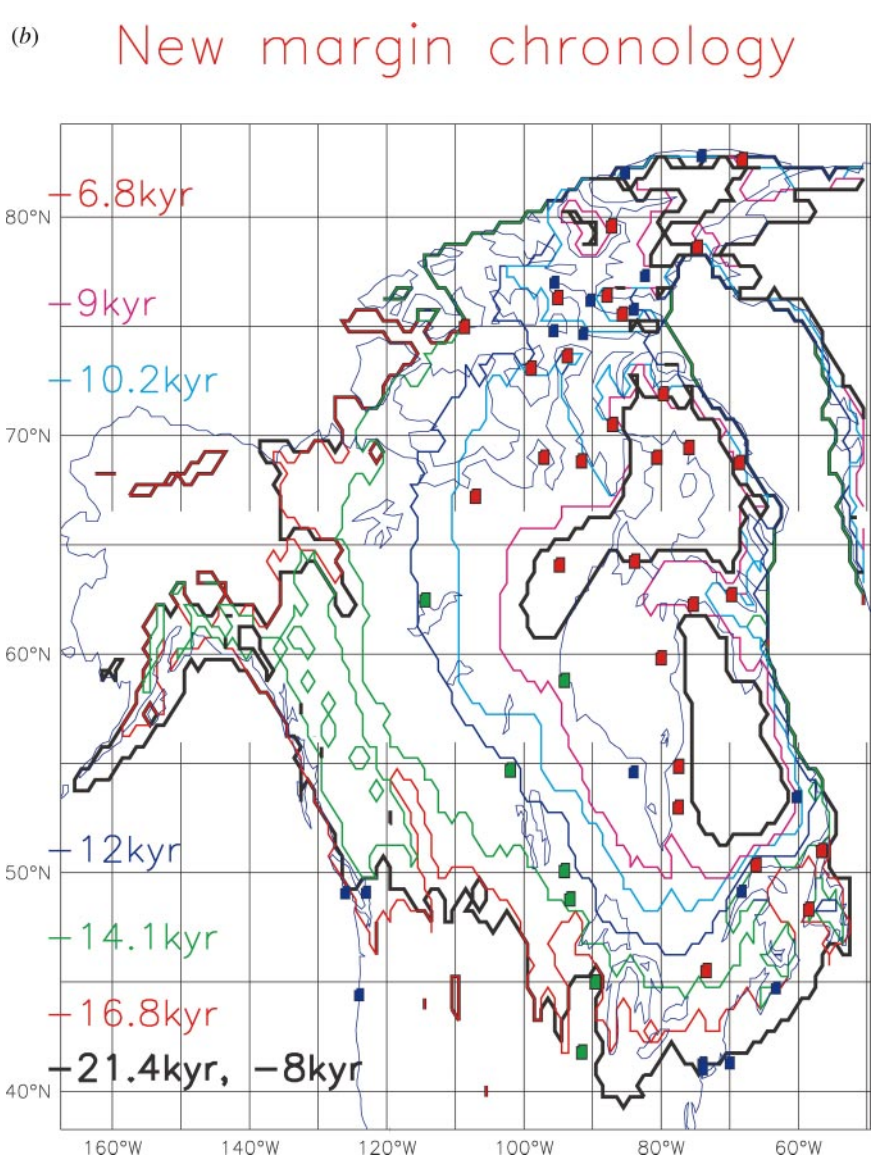

Figure 19 (*Continued*)

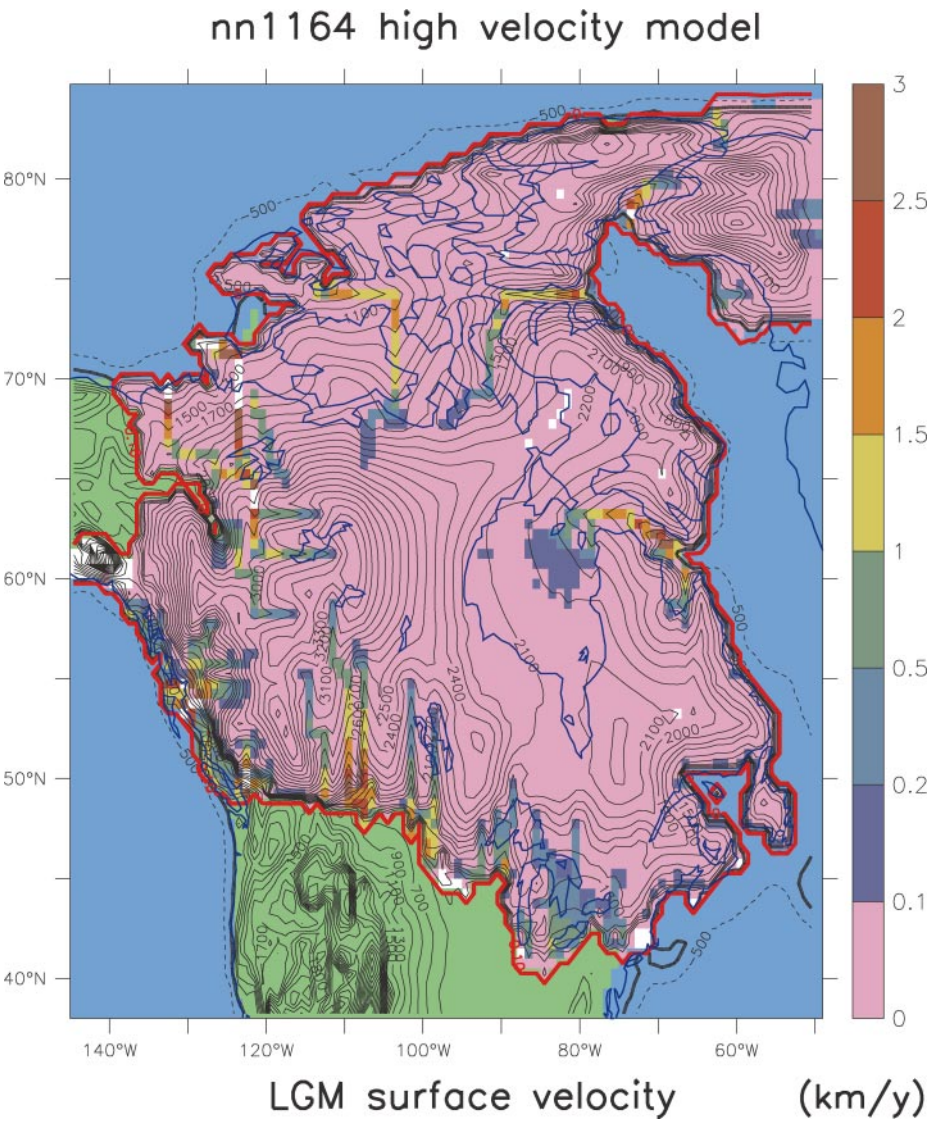

Figure 20 LGM isopacks of North American ice-sheet thickness superimposed upon a color-coded depiction of the speed of ice-sheet flow. Note the presence of the highly developed Hudson Strait ice stream and the relative minimum of topography over Hudson Bay itself that is produced by the down-draw owing to the fast-flowing stream. Note also the plethora of ice streams that have developed on the southern flank of the ice complex over the region where sediment thickness is appreciable according to the map shown in Figure 19*a*. Of primary importance, however, are the three regional domes of ice that are predicted to develop over the exposed crystalline basement in the Keewatin sector of the Shield centered upon Yellowknife to the southeast Hudson Bay, and less, obviously, in the Foxe Basin to the west of Baffin Island.

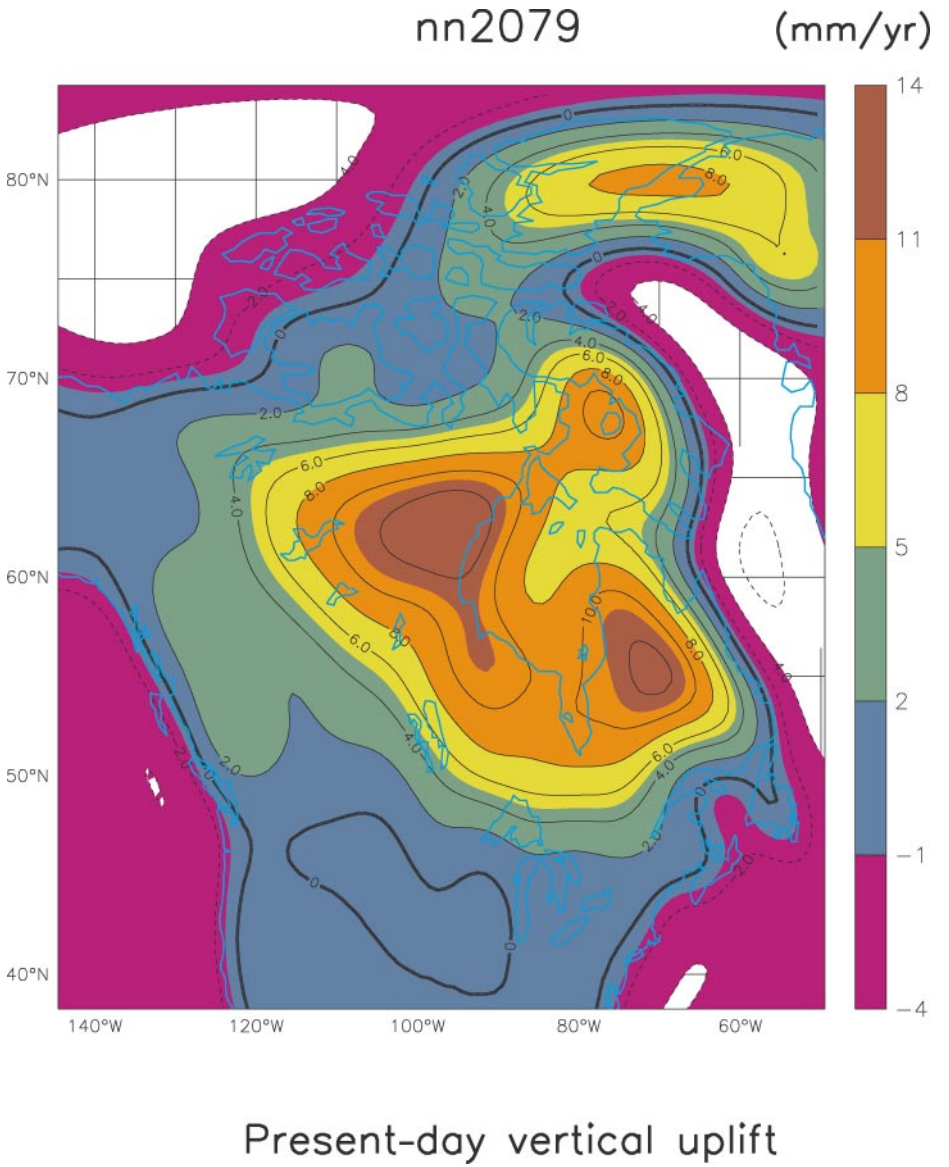

Figure 21 ICE-5G (VM2) prediction of the present-day rate of vertical motion of Earth's crust over the North American continent. Notable are the three centers of maximum uplift associated with the three primary domes of the ice complex.

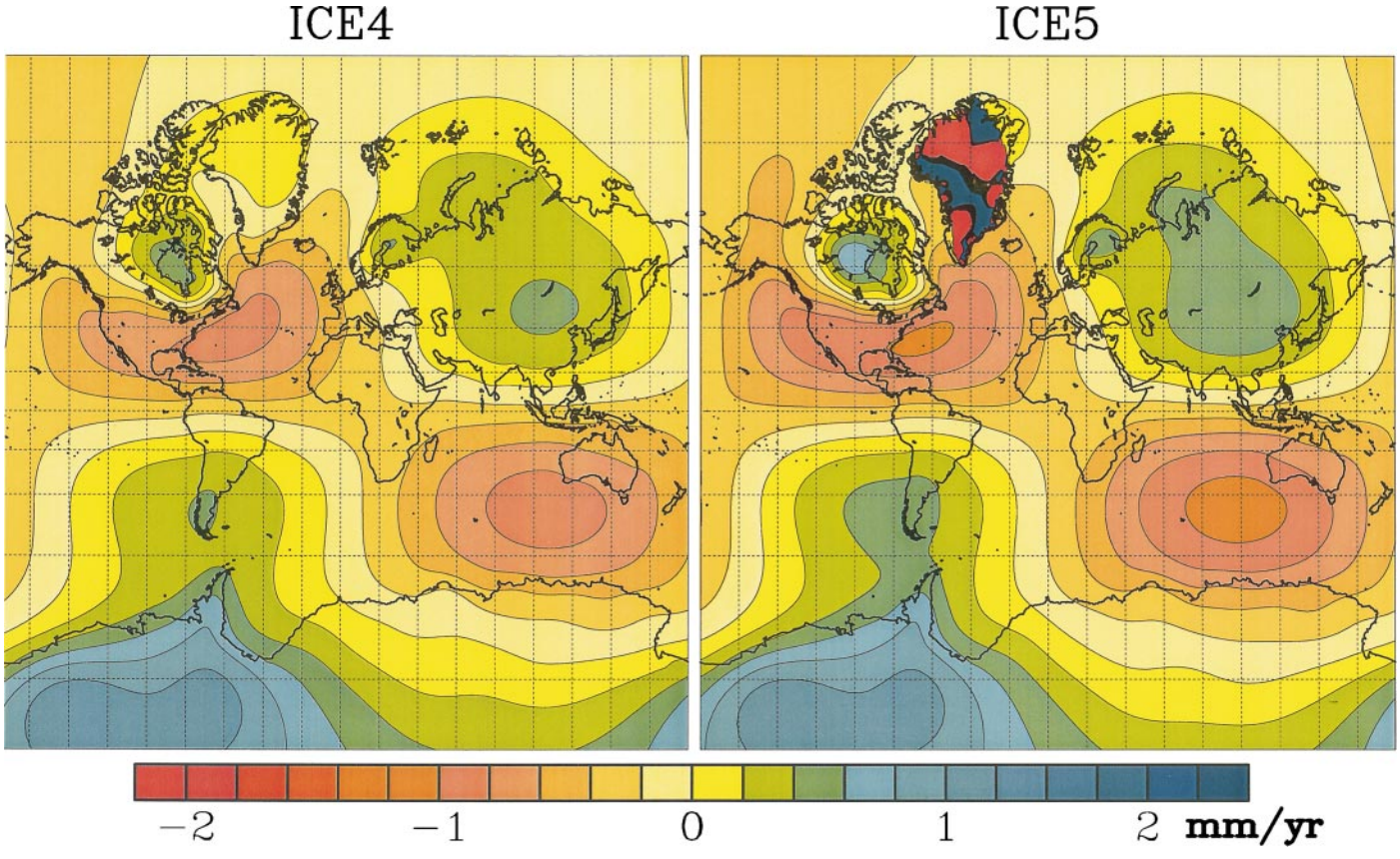

Figure 22 Present-day geoide height time dependence predicted by (*a*) the ICE-4G (VM2) model and (*b*) the ICE-5G (VM2) model. The maps are shown in Mercator projection so as to emphasize the polar regions in which the differences are most extreme.

Annual Review of Earth and Planetary Science
Volume 32, 2004

CONTENTS